Title

Uncovering the transcriptomic heterogeneity of pancreatic endothelial cells using integrative and comparative single cell gene expression analysis

Authors

Safwat T. Khan[1], Neha Ahuja[2], Sonia Taib[3], Shabana Vohra[3], Ondine Cleaver[2], Sara S Nunes[1,3,4,5]*

Affiliations

[1]Institute of Biomedical Engineering, University of Toronto, Toronto, ON, Canada;
[2]Department of Molecular Biology and Center for Regenerative Science and Medicine, University of Texas Southwestern Medical Center, Dallas, TX, USA;
[3]Toronto General Hospital Research Institute, University Health Network, Toronto, ON, Canada;
[4]Laboratory of Medicine and Pathobiology, University of Toronto, Toronto, ON, Canada;
[5]Heart and Stroke/Richard Lewar Centre of Excellence, University of Toronto, Toronto, ON, Canada;
[6]Ajmera Transplant Center, University Health Network, Toronto, ON, Canada;

* Corresponding author:

Sara S. Nunes Vasconcelos

University Health Network,

101 College St. MaRS TMDT 3-904,

Toronto, ON, M5G 1L7

Canada.
Email address: sara.vasconcelos@utoronto.ca

Abstract

The pancreatic islet vasculature displays tissue-specific physiological and functional adaptations that support rapid glucose sensing and insulin response by β-cells. To uncover the transcriptomic basis of this specialization, we performed a meta-analysis of multi-organ single cell RNA sequencing atlases employing a unique strategy to avoid transcriptomic contamination. We identified biologically relevant genes involved in sphingosine-1-phosphate-mediated insulin-secretion (*PLPP1, RDX, CDC42*), islet basement membrane formation (*SPARC, COL15A1*), endothelial cell (EC) permeability (*PLVAP, EHD4*), membrane transporters (*CD320, SLCO2A1)* and developmental transcription factors (*NKX2-3, AHR)*. These were validated *in silico* in an independent dataset. We further established the first integrated transcriptomic atlas of human pancreatic ECs and described two unique capillary subpopulations: exocrine and endocrine pancreas ECs. We validated the spatial localization of key markers using RNAscope™ and immunofluorescence staining on mouse pancreatic tissue cross-sections. Our findings provide novel insights into pancreatic EC heterogeneity and islet EC function with potential implications in therapeutic strategies.

Teaser

Introduction of a biologically relevant pancreas-specific endothelial cell (EC) gene signature and integrated atlas of human pancreatic ECs.

MAIN TEXT

The manuscript should be a maximum of 15,000 words.

Introduction

Endothelial cells (ECs) are the interface for tissue-blood exchange of oxygen, nutrients, and metabolic waste products. ECs also secrete soluble factors, known as angiocrine factors, that are important for tissue morphogenesis, repair and homeostasis(*1*). Furthermore, ECs adopt unique tissue-specific characteristics to meet the functional needs of the surrounding parenchyma such as in the brain(*2*) and liver(*3*). Similarly, the pancreatic Islets of Langerhans are made up of several hormone-secreting cell-types, such as insulin-secreting β-cells and glucagon-secreting α-cells(*4*), which directly regulate blood glucose levels and are thus intimately connected to the vasculature. In fact, despite making up only 1-2% of the pancreatic mass(*5*), islets are densely vascularized and receive up to 10-20% of the blood volume to the pancreas(*6*, *7*). Pancreatic ECs also display pore-like structures, where the endothelium tapers off into a thin diaphragm, called fenestrations, which increase the permeability of small molecules across the endothelium and facilitate the exchange of factors between the blood and extravascular tissue. Compared to exocrine vasculature, the islet vasculature is known to have ~10 times the number of fenestrations(*5*). Importantly, an intricate cellular-cross talk between ECs and β-cells that is imperative for proper β-cell development, proliferation and insulin secretion has also been demonstrated *in vivo*(*8*, *9*). Furthermore, endothelial abberations in the islets has been implicated in the pathophysiology of both type 1 and type 2 diabetes mellitus(*10*, *11*). However, the specific mechanism whereby islet fenestrations are formed, how islet ECs mediate insulin-glucose transport and their role in diabetes is not well understood.

The recent use of single cell/nucleus RNA sequencing (scRNAseq/snRNAseq) technologies, has allowed major advances in the characterization of tissue-specific endothelial signatures for various organs (*12*, *13*). However, there is limited data available for islet ECs. This is because the exocrine pancreas is primarily composed of acinar cells, which secrete high levels of hydrolytic enzymes. When the whole pancreas is dissociated into single cells/nuclei, these enzymes interfere with sequencing data. As a result, the majority of the pancreas datasets have sequenced isolated, *in vitro* cultured islets(*14–19*) and the ECs do not survive this process(*20*). Altogether pancreas/pancreatic islet datasets with a substantial, viable EC population is difficult to obtain.

Furthermore, comparison of the gene expression of pancreatic ECs to other pancreas cells, does not allow for extracting information regarding endothelial specialization. For this purpose, it is more relevant to compare pancreatic ECs to ECs in other tissues and identify differences within pancreatic ECs, i.e. between exocrine and endocrine (islet) ECs.

Integrating EC data from numerous publically available studies that have sequenced different organs is challenging. This is because any downstream analysis is highly susceptible to the sequencing library preparation technique(*21*) making it difficult to ascertain actual biological gene expression differences from that conjured by batch-effects. Therefore, for an unbiased comparison between different tissue EC sequencing data, they must be acquired using the same methodology. As such, we have looked towards multi-organ gene expression atlases, which sequenced and aligned all tissues under a standardized workflow.

Kalucka et al.(*22*) has generated one such comprehensive EC-specific murine gene expression atlas, unfortunately it does not contain pancreas ECs. Other studies(*23*, *24*) have also generated organotypic signatures for ECs by subsetting only ECs from the Tabula Muris atlas(*25*), which contains scRNAseq data on ~ 100,000 adult mouse cells generated using the FACS-based SmartSeq2 assay. However, they identified acinar-specific genes as top pancreas-specific EC

genes, including genes such as *CPA1, CLPS, CEL, CELA3B, CTRBB1* and *PNLIP*. This highlights an issue of RNA contamination, which likely results from the aforementioned lysis of acinar cells during single cell dissociation.

Therefore, to define a biologically relevant pancreas-specific EC gene signature we have analyzed ECs subsetted from two different multi-organ atlases, the aforementioned adult mouse Tabula Muris and the human fetal Descartes (*26*). We use these two multi-organ atlases to generate their respective EC-only atlases and then determine a cross-atlas conserved pancreas-specific EC gene signature. We validate this signature *in silico* on a third EC atlas, obtained from the Tabula Sapiens(*27*). Further, to avoid misidentifying ambient contaminant genes as pancreas-specific EC genes, we curated a list of endothelial-specific genes by analyzing four pancreas scRNAseq/snRNAseq datasets, which we then use to cross-reference discovered gene lists with. Using our analysis pipeline, we identify genes that are enriched in pancreas ECs compared to other tissue ECs, across three different multi-organ gene expression atlases. Top genes of interest identified are involved in processes coherent with islet endothelial functions, such as sphingosine-1-phosphate mediated insulin secretion (*PLPP1, RDX, CDC42)*, islet basement formation (*SPARC, COL15A1)*, endothelial barrier integrity *(HEG1)*, vascular permeability *(PLVAP, EHD4)* and membrane transport *(CD320, SLCO2A1)*. In addition, we introduce the first integrated human pancreatic EC atlas derived from three human datasets and dissect pancreatic EC heterogeneity. Using this integrated atlas, we described and valiated *in situ* the existence of transcriptomically distinct endocrine-specific and exocrine-specific capillary subpopulations. Our approach provides a comprehensive overview of the inter and intra-tissue transcriptomic landscape of pancreatic ECs. This will help us better understand the role of islet microvessels in regulating glucose homeostasis and advance research in diabetes therapy.

Results

Comparative analysis of multi-organ gene expression atlases to define a pancreas-specific gene signature for endothelial cells.

To generate a transcriptomic profile of pancreatic ECs, we have conducted comparative analysis against other tissue ECs using multi-organ gene expression atlases and integrated human pancreatic EC sequencing data to dissect the inter and intra-tissue pancreatic endothelial heterogeneity respectively (Figure 1). To define a pancreas-specific endothelial gene signature, we subsetted and pooled all cells previously annotated as endothelial by the studies' respective authors, from all available organs from the Tabula Muris and Descartes atlases (Table 1). This generated an EC atlas for fetal human tissue and adult mouse tissue (Descardes and Tabula Muris), respectively(Figure 2 A-F). We then identified differentially expressed genes (DEGs) (log2FoldChange > 0.25) enriched in pancreas ECs compared to ECs from all other tissues for each atlas (Figure 2C and 2F). This generated a list of pancreas-enriched DEGs from the Descartes and the Tabula Muris EC atlases (Supplementary Table 1 and 2). However, closer inspection of these DEGs revealed a significant number of acinar and endocrine-specific genes, likely resulting from ambient RNA contamination from surrounding exocrine and endocrine genes(*28*). While there have been notable tools developed that can tease out ambient RNA expression such as SoupX(*29*) and DecontX(*30*), their methodologies depend on detecting ambient RNA that is expressed in all cell-types obtained from the same sample. However, when comparing ECs across tissues that were isolated and sequenced tissue-by-tissue, the ambient RNA contamination present in pancreatic ECs is not present in the other tissue ECs. As such, the contamination DEGs could be identified as *de novo* genes. Therefore, we chose to not use *SoupX* or *DecontX*.

Instead, to avoid selecting these contaminant genes in downstream analyses, we sought to curate a list of endothelial-specific genes with which to cross-reference the pancreas-enriched DEGs from Descartes and Tabula Muris EC atlases. To do so, we analyzed four different pancreas datasets.

These include the scRNAseq pancreas dataset from the Descartes and Tabula Muris gene expression atlases as well as a human adult and a human neonatal snRNAseq pancreas datasets generated by Tosti et al.(*31*) (henceforth referred to as Tosti-Adult and Tosti-Neonatal, respectively) (Table 1, Supplementary Figure 1 and 2). For each dataset, we identified the significant DEGs (log2FoldChange > 0.25, Bonferroni-adjusted p-value < 0.05) enriched in the pancreatic vascular EC populations against all other non-vascular pancreatic populations, such as β-cells or acinar cells, excluding lymphatic ECs and perivascular cells, which could have overlapping gene expression with ECs (Supplementary Table 3).

We reasoned that any remaining DEGs that are upregulated in ECs cannot be contaminating genes from other populations, as the contaminating genes should have a higher expression in the cell-type it originates from. We observed limited overlap in the endothelial genes discovered in the four datasets. This highlights both biological variability, as well as technical variability in generating these datasets. However, it also highlights the ability of each dataset to detect unique endothelial genes in the pancreas that cannot be detected in the sample type or by the methodology used in the other datasets. As such, to ensure our list does not exclude potential endothelial genes, we merged all 1,996 unique DEGs identified from the four datasets into one list (Figure 2G). We refered to these DEGs as the list of endothelial-enriched DEGs.

Next, we cross referenced the pancreas-enriched DEGs from the EC atlases (Descartes and Tabula Muris) with the list of endothelial-enriched DEGs (Figure 2F) (Supplementary Table 4 and 5) and removed any genes that did not overlap with this list. This demonstrated that most of the top EC DEGs, are contamination in both atlases (Figure 3A and B). Among the remaining DEGs, we identify 87 genes which were common between all three lists. This indicates that they are highly conserved and potentially relevant, as they were identified irrespective of species (mouse and human), sequencing method (FACS-based and droplet-based) and age (adult and fetal). We refer to these 87 genes as the 'pancreas-specific EC gene signature' (Table 2). Hierarchical clustering of the different organ ECs based on the expression of signature DEGs allowed pancreas ECs to cluster separately, in its own branch, in both the Descartes and Tabula Muris EC atlas (Figure 3C and D). To further increase confidence in the biological relevance of this gene signature, we assessed its expression in an independent, third multi-organ atlas, i.e. not used to derive this signature.

Validation of pancreas-specific EC gene signature in an independent multi-organ atlas

For this purpose, we analyzed the adult human Tabula Sapiens gene expression atlas. Its corresponding EC atlas was generated by subsetting all annotated ECs, similarly to the Descartes and Tabula Muris EC atlases (Figure 4A-B). We then assessed the collective expression of the pancreas-specific EC signature genes using Seurat's module score(*32*), which employs the scoring strategy described by Tirosh, et al(*33*). We showed that the module score for the pancreas-specific EC signature was highest in the EC population in the pancreas, compared to other EC populations in all other tissues (Figure 4C), confirming pancreas specificity of the gene signature. Hierarchical clustering based on average scaled expression of the signature DEGs, also clustered pancreas ECs separately from all other organ ECs (Figure 4D). Additionally, individual gene expression patterns demonstrated that not all signature genes were uniquely expressed in pancreatic ECs. In fact, single cell omics analysis has revealed many genes previously assumed to have organ-specific endothelial expression are still expressed in EC in other tissues but to a lesser extent(*22*). We found that it is a unique collective gene expression signature that is specific to pancreas ECs, rather than the expression of individual genes. Here we validated *in silico* several genes in our list of signature genes to be highly enriched in pancreas ECs compared to other tissue ECs in the Tabula Sapiens EC atlas. We have also confirmed the vascular expression of several of these genes (*Nkx2-3, Plcb1, Clec14a, Heg1*) *in situ* in the pancreas of E18.5 mouse pancreas (Figure 4E).

When we sorted the signature genes based on fold-change in percentage of pancreas ECs expressing the gene against other tissue ECs, the homeobox sequence containing *NKX2-3* was the top differentiative gene. *NKX2-3* is a developmental transcription factor (TF) that has been shown to regulate the expression of several key endothelial genes(*34*). This gene was also one of the top differentiative gene in both the Descartes and Tabula Muris EC atlas (Figure 3C and D). Another TF validated *in silico* to be enriched in pancreatic ECs is Aryl hydrocarbon receptor (*AHR*), which is involved in vascular development(*35*) and angiogenesis(*36*). *AHR* is also and involved in S1P signalling(*37*), which in turn has been shown to be involved in glucose-stimulated insulin secretion(*38*, *39*).

Importantly, we also observe several genes potentially involved in S1P-mediated regulation of endothelial barrier integrity via the Rho GTPase signalling pathway. For example, there is enrichment of the Cdc42 effector protein (*CDC42EP1*), which binds to Cdc42 a member of the Rho family of GTPases. We also see enrichment of Radixin (*RDX*) which is part of the ERM (Ezrin-Radixin-Moesin) family of actin-binding proteins and integral for S1P-mediated endothelial barrier integrity(*40*). We also observe other cytoskeletal genes such Synaptopodin (*SYNPO*) and Refilin B (*RFNLB* or *FAM101B*) enriched in pancreas ECs, which is consistent with cytoskeletal alterations induced by S1P. Other genes related to S1P-mediated endothelial barrier regulation, which were not expressed in the Tabula Sapiens but were still present in our signature gene list, i.e. they were pancreas-specific in Tabula Muris and Descartes EC atlas include; moesin (*MSN*), another ERM actin-binding protein(*40*) and *SPNS2*, a S1P transporter protein.

We further assessed the expression of other proteins directly involved with S1P-signalling across all ECs and across all cell-types in the pancreas in the Tabula Sapiens (Figure 5A). This include sphingosine kinases (*SPHK1, SPHK2*), which phosphorylate sphingosine to form S1P, all S1P-receptors (*S1PR1-5*) and phospholipid phosphatases (*PLPP1-3*), which dephosphorylates S1P back to sphingosine(*41*). Interstingly, β-cells do not notably express any of these genes directly, while pancreatic ECs highly express *S1PR1* and *PLPP1* . In fact, *PLPP1* had the highest expression in pancreas ECs across all tissue ECs. *S1PR1*, was also highly expressed in pancreatic ECs however, it had the highest expression in heart ECs.

CDC42 is also involved in insulin-signaling mediated glucose transport(*42*) and protein kinase N1 (*PKN1*), which is a key Rho-mediated kinase involved in transmitting insulin signaling to the actin cytoskeleton, was also enriched in ECs of the pancreas(*43*, *44*). Other genes of interest that were validated *in silico* include; heart-of-glass protein (*HEG1*) involved in vascular junctional integrity(*45*); plasmalemma vesicle associated protein (*PLVAP*), the widely used marker of endothelial fenestration(*46*); EH-domain containing 4 (*EHD4*), which is involved in the formation of caveolae(*47*), which are invaginations on the endothelial wall involved in transport; *COL15A1*, which has been shown to be expressed in a novel venous population, specific to the visceral pleura in the lung(*12*, *48*); and *CLEC14A*, which is an important endothelial cell-cell adhesion molecule(*47*).

We further analyze all pancreas-enriched EC genes in the Tabula Sapiens EC atlas. Similar to the other EC atlases, the top DEGs were contaminating genes (Figure 5B, Supplementar Table 6). As before, to avoid contaminating genes, we cross-referenced these DEGs with the curated list of endothelial-enriched DEGs. In total, among all the pancreas-enriched DEGs from the Tabula Sapiens EC atlas, 366 DEGs were also endothelial-enriched (Figure 5C). We then compared these with the DEGs from the Descartes and Tabula Muris EC atlases. Overall, 36 DEGs overlapped across all 3 lists (Table 2, Figure 5D) and include the genes described previously.

239 Beyond these genes of interest, there were also genes that only overlaped between the human
240 Descartes and Tabula Sapiens EC atlases, but not the mouse Tabula Muris EC atlas. This may
241 constitute human-specific pancreas-enriched EC genes. In total 105 genes, uniquely overlapped
242 between pancreas-enriched DEGs from the Descartes EC atlas and the Tabula Sapiens EC atlas
243 (Figure 5D and E). The top 10 DEGs by log2FC in pancreas ECs against other pancreatic cells
244 from this list in the Tabula Sapiens EC atlas include; a transcobalamin transporter (*CD320)*, which
245 is involved in the transcytosis of vitamin B12(*49*); a prostaglandin transporter (*SLCO2A1*)(*50*);
246 insulin-like growth factor binding protein 4 (*IGFBP4*); transmembrane Protein 88 (*TMEM88),* an
247 inhibitor of the Wnt/β-catenin signaling pathway implicated in proper cardiovascular development
248 (*51*); thioredoxin interacting protein (*TXNIP*), which is involved in *VEGF* signalling(*52*); a
249 member of the major histone compatibility (MHC) complex, *HLA-C*; *SPARCL1* or Hevin, a
250 member of the SPARC family of matricellular proteins(*53*), involved in angiogenesis, vessel
251 integrity(*54*), vascular permeability(*55*) and glucose homoestasis(*56*); a member of the SOX-
252 family of TF (*SOX18*), which is integral in vascular development(*57*); and *FAM13C*, which is an
253 understudied protein.

254 Potentially identifying adult-specific pancreas EC genes, we found 59 DEGs also overlapped
255 uniquely between the two adult atlases, Tabula Sapiens EC atlas and Tabula Muris EC atlas, but
256 not the fetal Descartes EC atlas. The top 10 DEGs by log2FC in pancreas ECs against other
257 pancreatic cells from this list in the Tabula Sapiens EC atlas include; TGFβ Type 2 receptor protein
258 (*TGFB2R*), which binds TGFβ, an important regulator of endothelial function(*58*); *PLPP1*, which,
259 as we describe previously, dephosphorylates S1P to sphingosine(*41*); integrin alpha-1 (*ITGA1)*, an
260 important islet basement membrane protein(*59*); growth arrest-specific protein 6 (*GAS6)* involved
261 in angiogenesis(*60*); G protein-coupled receptor 146 (*GPR146)*, involved in vascular
262 remodelling(*61*); cellular communication network factor 2 (*CCN2)* an ECM protein important for
263 pericyte adhesion(*62*); atonal BHLH TF 8 (*ATOH8)*, which is an important TF for endothelial
264 cells(*63*) and embryonic pancreas development(*64*); VEGF receptor 2 (*KDR*); and *FAM167B*,
265 another understudied protein. The remaining 166 DEGs that are only specific to Tabula Sapiens
266 are also of interest, as these could include novel genes that cannot be detected due to the limitations
267 of the other two atlases (Supplementar Table 6).

268 **Defining the intra-tissue endothelial heterogeneity in the pancreas**

269 Next, we assessed the intratissue EC heterogeneity in the pancreas. To maximize our transcriptomic
270 resolution, we used Harmony(*65*) to integrate the pancreatic ECs across the 3 human datasets.
271 These include the fetal pancreas EC data from Descartes (Descartes-Fetal), Tosti-Adult and Tosti-
272 Neonatal (Figure 6A). Read count matrices for ECs from each dataset were preprocessed, log-
273 normalized and clustered as described in the methods section. Unsupervised clustering revealed
274 several contaminating clusters within each pancreatic EC dataset, which did not express canonical
275 endothelial genes (*CDH5, KDR, VWF*) or had co-expression of non-endothelial contaminating
276 genes. To ensure these populations did not interfere with proper integration of pancreatic ECs
277 across datasets, the contaminating clusters were removed prior to integration. As a result, 3,857
278 ECs, 1,023 ECs and 576 ECs were used for integration from the Descartes-Fetal, Tosti-Adult and
279 Tosti-Neonatal datasets, respectively.

280 This produced an atlas of human pancreatic ECs with 6 different subpopulations. These unique
281 populations were present in approximately equal proportions across the individual datasets (Figure
282 6B and C). Based on gene expression patterns, we discovered that these populations corresponded
283 to the topographical location of ECs along the vascular tree (Figure 6D). Three arterial populations
284 were identified by the expression of *GJA5*(*66*) *GJA4* (*67*) and *EFNB2* (*68*). Artery 1 population

was additionally enriched for elastin (*ELN*) and *SULF1*, which are involved in artery extracellular matrix (ECM) formation(*69*). The arteriole population had co-expression of arterial markers and *CD36*, which has also been shown to be differentially expressed in capillary ECs in the lung(*12*). *CD36* was also highly expressed in the two capillary populations, capillary 1 and capillary 2, alongiside *PLVAP* and *COL15A1*. We also annotate one venule population based on the expression of the venule marker *DARC* (*70*). When we calculated module scores based on the collective expression of the pancreas-specific EC signature genes derived previously, we saw that capillary 1, had the highest module score for this signature, followed by the arteriole population (Supplementary Figure 4).

DE analysis (Supplementary Table 7) between the different subpopulations revealed genes involved in caveolae and fenestrae formation, ECM production, insulin-like growth factor (IGF) signalling, SOXF transcription factors, immune-activity, and membrane transport. Therefore, we assessed other genes in these families, to identify potential trends that correspond to the vascular hierarchy (Figure 6E). Notably, compared to capillary 2, capillary 1 had higher expression of several caveolae and fenestrae associated genes such as *PLVAP*(*71*), *SDPR* (or *CAVIN2*)(*72*) and *EHD4*(*73*). It also had higher expression of several immune-related genes, including *FABP5*(*74*) and *CD74*(*75*), which are involved in inflammation in macrophages and several major histocompatibility complex (MHC) proteins such as *ITM2A, B2M, HLA-C, HLA-B*. Higher immunological activity and presence of fenestrae are characteristics that have previously been attributed in literature to intra-islet capillaires in comparison to exocrine capillaries(*76*). This suggests that capillary 1 and capillary 2 subpopulations are islet capillary ECs and exocrine capillary ECs, respectively. Other genes highly enriched in capillary 1 included *SPARC,* and its structurally similary counterpart *SPARCL1*, which are matricellular proteins involved in angiogenesis(*54*), vascular permeability(*55*) and implicated in glucose homeostasis(*56*); *IGFBP7*, a secreted factor stored in Weibel-Palade bodies(*77*), which has been implicated in angiogenesis and vascular permeability(*78*); the prostaglandin transporter, *SLCO2A1*; vitamin B12 transporter *CD320,* and the glucose transporter, *SLC2A3*. Importantly, many of these genes overlapped with the pancreas-enriched EC genes identified previously (Table 2, Supplementary Table 4 and 5). By contrast, capillary 2 displayed a more generic expression pattern with no significantly enriched genes compared to capillary 1. The arteriole population also had an interesting gene expression pattern, as it had the highest expression of *HEG1*, which is involved in barrier integrity(*45*); *SOX7*, which is another SOX-TF involved in vascular development and shown to be highly expressed in arterioles(*79*); insulin-like growth factor binding protein 3 (*IGFBP3)* and insulin receptor (*INSR)*, which are major components of the insulin and IGF signalling pathways.

We also performed pseudotime trajectory inference of the integrated pancreatic EC map on the UMAP space using SCORPIUS, a machine learning tool which has been benchmarked to be one of the best trajectory methods based on overall performance(*80*) (Figure 6F). The analysis predicted a trajectory from the venule population to the artery populations, through the capillary populations. This further supports the capillary annotation. Gene expression of top markers (Supplementary Table 7) for each vacular bed subpopulation across pseudotime also demonstrated a continuous gene expression pattern across the vascular topography rather than discrete endothelial subpopulations (Figure 6G). We also identify genes that predict the ordering of the cells along pseudotime, ranked by an importance score derived using a Random Forests algorithm employed by SCORPIUS (Figure 6H). This allowed us to identify the expression pattern of both established (*GJA4, GJA5, DARC*) and under studied arterio-venous markers for differentiating ECs along the vascular tree. Of these genes, we found that capillaries have peak expression of *PLVAP* and *APLNR*, which has been implicated in apelin-mediated glucose control. Another gene of interest is *UNC5B*, which shows peak expression in the arteriole ECs, and has been recently shown to regulate blood-

brain barrier integrity through interaction with netrin-1(*81*). Several other genes (*POSTN, GPR126* and *ZNF385D)* match the expression pattern of *DARC*, which peaks specifically in Venule ECs, suggesting these could be novel marker genes for venous ECs, at least in the pancreas.

Validation of an islet-specific EC cell population

Next, we applied a cell-type annotation transfer mapping method on the Tabula Sapiens pancreas ECs, using the integrated pancreatic EC atlas as the reference (Supplementary Figure 5). Three different subpopulations were identified in the Tabula Sapiens: artery 2, capillary 1 (islet capillary) and the venule subpopulations. These annotations were corroborated by assessing the expression of marker genes *GJA4, CD36* and *DARC* (or *ACKR1*) in these clusters. The majority of the cells were annotated as capillary 1. No capillary 2 ECs were annotated. This is still consistent with our annotation of capillary 2 as exocrine capillary endothelial cells, which are likely to be damaged during the enzymatic digestion process used to sequence pancreas tissue in the Tabula Sapiens.

Finally, to validate that th transcriptomic signature for capillary 1 and capillary 2 in the integrated map correspond to EC populations in the endocrine (or intra-islet) and exocrine capillaries respectively, *in vivo*, we assessed the expression of 3 DEGs, *PLVAP, SPARC*, and *NKX2-3*, which were enriched in capillary 1 against all other subpopulations, including capillary 2, in the integrated atlas (Figure 7C). We conducted RNAscope™ and IF staining of these genes *in situ* on E18.5 mouse pancreatic tissue (Figure 7D). RNAscope™ data demonstrated that a large portion of the probes, 70.1% (± 3.44 %) for *Sparc* and 49.6% (± 5.44 %) for *Nkx2-3,* were co-localized within the vessels (Figure 7E). This is consistent with our analysis that demonstrate NKX2-3 is also expressed by stellate cells (Supplementary Figure 3). IF staining and quantification of *Plvap* showed that it had over 2 times as higher fluorescence intensity (3970AU ± 571) in endocrine *Pecam1/Endomucin*$^{+}$ capillaries compared to exocrine capillaries (1513 AU ± 268) (Figure 7F). Further, *Sparc* in the endocrine vessels had over 3 times as much RNA expression level as measured by area of bound probe (0.0416 μm^2 ± 0.0086) compared to the exocrine vessels (0.01234 μm^2 ± 0.0012) (Figure 7F). RNAscope™ of *Nkx2-3* did not show any statistical difference in endocrine vs exocrine vessels, however, the mean area of probe binding was higher within the islets. Overall the expression pattern of endocrine and exocrine capillary ECs, further corrobate our capillary annotation for the integrated pancreatic EC map.

Discussion

Endothelial cells demonstrate a remarkable extent of intra and inter-tissue heterogeneity in structure, function, and molecular characteristics. With the advent of omics technologies, it is now possible to dissect this organotypic heterogeneity down to the single cell resolution. Here we have analyzed different multi-organ gene expression atlases and have established a unique, cross-species conserved, *in silico* and *in situ* validated pancreas-specific EC gene signature. This signature included genes involved in insulin-secretion, fenestrae and caveolae formation, islet basement membrane components, endothelial barrier integrity, vascular permeability and key developmental TFs. Furthermore, we have established the first integrated atlas of human pancreatic ECs using three recently published human pancreatic EC datasets from fetal, adult and neonatal human samples. This is similar to previously generated integrated atlases for ECs in the brain(*13*) and lung(*12*) and allowed us to identify distinct subpopulations with unique gene expression patterns, corresponding to the topographical location of ECs along the vascular tree. Specifically, we describe two unique capillary subpopulations, which we validated *in situ* to correspond to endocrine (intra-islet) and exocrine capillary endothelial populations.

The importance of profiling the transcriptomics of pancreatic ECs is clear when considering the integral nature of ECs in β-cell development and function, and its relevance in diabetes. The

379 pancreas-specific EC gene signature can shed insight into the development of specialization in
380 glucose homeostasis and insulin transport within the islet microvasculature. Further, owing to the
381 tissue-specific roles of ECs, there is a recent push towards generating induced pluripotent-stem cell
382 (iPSC)-derived organotypic ECs for tissue-specific vascular regeneration, and building
383 physiologically relevant 3D vascularized tissue models *in vitro*, which remains an outstanding
384 challenge in regenerative medicine(*82*, *83*).

385 Past attempts at generating a transcriptomic signature of pancreatic ECs have inadvertently
386 introduced bias(*23*, *24*) from contaminating/ambient RNA from lysed acinar cells, which skewed
387 the differential expression analysis. To circumvent this issue and uncover a contaminant-free, gene
388 signature for pancreatic ECs, we have cross-referenced the pancreas-specific EC genes with a list
389 of endothelial-enriched markers in the pancreas, i.e. they are expressed in ECs and not by possible
390 contaminating populations such as endocrine and exocrine cells. It is worth mentioning that two
391 different endothelial gene expression atlases (Descartes and Tabula Muris EC atlas) were used to
392 derive the pancreatic EC-specific signature, which was then *in silico* validated on a third,
393 independent gene expression atlas, the Tabula Sapiens EC atlas. We also validated gene expression
394 *in situ*, confirming the expression of several of the signature genes within the ECs of the pancreas.
395 Altogether, this increased the confidence that the observed gene expression patterns are
396 representative of genuine biological processes in the pancreatic microvasculature.

397 Specifically, we identified and validated *PLVAP*, which encodes for plasmalemma vesicle-
398 associated protein that is present in the the diaphragms of endothelial fenestrae and in caveolae
399 (*71*), as being highly enriched in pancreatic ECs. This is true even when comparing to other
400 fenestrated ECs such as of the kidney. *PLVAP* was also enriched in capillary 1 ECs compared to
401 all other EC populations in the integrated atlas, including capillary 2. Consistent with this, PLVAP
402 protein expression was validated *in situ* to be significantly higher in endocrine capillaries compared
403 to exocrine capillaries. This indicated that capillary 1 was the endocrine population and capillary 2
404 was the exocrine population. In the integrated atlas, *SDPR* (or *CAVIN2*) and *EHD4* were also
405 enriched in capillary 1 ECs compared to all other EC populations. *EHD4* was also identified in our
406 pancreas-specific EC gene-signature. *SDPR* directly regulates caveolae formation and morphology
407 (*72*) and *EHD4* colocalizes on the surface of caveolae(*73*). Altogether, this data shows higher
408 concentration of caveolae and fenestrae in endocrine pancreatic ECs compared to exocrine ECs as
409 well as other tissue ECs. This is functionally consistent with previous reports implicating caveolaes
410 in insulin and glucose transport(*84–86*).

411 Importantly, one of the top genes of interest across all three EC atlases was *NKX2-3* – which we
412 validated *in situ* and showed that it was indeed expressed in the EC in the pancreas. *NKX2-3* also
413 had higher expression in endocrine capillary ECs compared to exocrine capillary ECs in the
414 integrated pancreas EC atlas. However, we were unable to confirm that *NKX2-3* was enriched in
415 endocrine capillaries using *in situ* hybridization. This could be due to the fact that only a fraction
416 of ECs in the capillary 1 population express high levels of *NKX2-3*, making it difficult to tease out
417 differences *in situ* between exocrine and endocrine vessels.

418 *NKX2-3* is a member of the NK2 family of homeobox-domain containing TFs. These are critical
419 organ-specific developmental TFs(*87*, *88*). *NKX2-3* in particular is involved in the development
420 of the spleen and gut(*89*), both of which arise from the endoderm, which also gives rise to the
421 pancreas. Specifically, *NKX2-3* has been shown to be integral for proper vascular specification in
422 these organs(*90*, *91*). Primarily, *NKX2-3* is involved in regulating the expression of mucosal
423 vascular addressin cell adhesion molecule 1 (MAdCAM-1)(*92*). MAdCAM-1 is a tissue-specific
424 adhesion molecule that facilitates the homing of leukocytes in vascular segments involved in
425 immune surveillance and inflammation, such as the high endothelial venules found in lymph nodes
426 and Peyer's patches of the small intestine(*93*, *94*). Interestingly, in this study MAdCAM-1
427 expression was also highly enriched in pancreas ECs in the fetal human Descartes EC atlas.

Beyond, MAdCAM-1, *NKX2-3* has also been shown to be involved in regulating expression of other important angiocrine factors such as endothelin-1, VEGF-A, adrenomedullin and endothelial nitric oxide synthase(*34*, *95*). Therefore, the identification of *NKX2-3* as a top DEG enriched in pancreas-ECs compared to all other tissue ECs across all three EC atlases, as well as the potential higher expression in islet capillary ECs compared to exocrine capillary ECs, makes *NKX2-3* TF an exciting target to study. Specifically, its role in pancreatic vascular specification should be further investigated.

We also see numerous genes enriched in pancreas ECs that are related to S1P signalling. S1P is a bioactive lipid, which is secreted by platelets, red blood cells and ECs(*95*), that has garnered much research interest due to its multifaceted role in embryonic development, organ homeostasis and disease pathogenesis(*96*). In the pancreas, vascular derived S1P is involved in pancreas development(*97*). Further, evidence suggests that extracellular S1P may induce glucose-stimulated insulin secretion in β-cells(*38*, *39*). In fact, exogenous S1P has been shown to improve β-cell proliferation in a type 2 diabetic mouse model(*98*). In this study, we highlight several genes involved in S1P signalling, such as *AHR* and *RDX*, which were pancreas enriched across all three EC atlases, and *MSN, SPNS2* and *PLPP1*, which were pancreas enriched across at least two EC atlases. *AHR*, which encodes the Aryl Hydrocarbon Receptor, is a TF that has been implicated in regulating S1P bioavailability(*37*, *99*). *RDX* (Radixin) and *MSN* (Moesin), are members of the ERM-actin binding complex and are integral in S1P-mediated endothelial barrier permeability(*40*). *SPNS2*, is a S1P transporter(*41*) and *PLPP1* dephosphorylates S1P. Taken together, these findings suggest that pancreatic ECs play a critical role in the production, transport, and metabolism of S1P. Notably, S1P receptor genes (S1PR1-5) were not detected in β-cells across all pancreas datasets, whereas pancreas ECs highly expressed *S1PR1* compared to other pancreas cell-types. Thus, we hypothesize that S1P signaling primarily involves the islet ECs, which then propagates its effects to β-cells through other means to regulate their function. Further research is needed to fully elucidate the role of S1P and its associated proteins in the β-cell/EC axis.

Another pancreas EC enriched gene of interest is *SPARC*, also known as osteonectin, which is a member of the SPARC-family of matricellular proteins. Unlike conventional ECM proteins, matricellular proteins are non-scaffolding components of the ECM that are involved in a myriad of diverse and complex biological functions(*100*) such as regulating ECM remodelling, cell-matrix interactions and growth-factor activity. Importantly, it has been demonstrated *in vivo* that SPARC may regulate β cell growth(*101*) and insulin secretion(*102*) and is essential for proper glucose homeostasis in a type 2 diabetic mouse model(*56*). Further, *SPARC* expression was found to be differentially expressed in the islets and in the plasma of diabetic patients(*103*, *104*). Here, we demonstrated that *SPARC*, and another member of the family, SPARC-like protein 1 (*SPARCL1),* also known as hevin, are enriched in pancreatic ECs in the Tabula Sapiens EC atlas. *SPARC* and *SPARCL1* expression were also enriched in pancreas vascular ECs compared to all other pancreas cell-types, although stromal cells also expressed both genes as previously reported(*101*). Further, in the integrated pancreatic EC atlas, we observed enrichment of *SPARC* in endocrine capillary ECs compared to the exocrine capillary ECs. *In situ* validation in E18.5 mouse pancreatic tissue confirmed that islet capillaires had significantly higher *Sparc* expression.

Further, according to the integrated atlas, islet capillary ECs had higher expression of the vitamin B12 transporter *CD320*, prostaglandin transporter, *SLCO2A1* and glucose transporter *SLC2A3* (or *GLUT3*). *CD320* was also enriched in pancreas ECs in both human atlases. Therefore, the role of vitamin B12 and prostaglandin should be further investigated in pancreatic ECs. As these genes encode for membrane associated proteins, they could also act as potential biomarkers for islet capillary ECs along with the caveolae and fenestrae associated genes *PLVAP, EHD4* and *SDPR*.

Finally, we identified an arteriole population, which had enrichment of *IGFBP3* and *INSR* compared to the other EC populations in the integrated atlas. This indicated potentialy important roles in insulin-signalling in the arterioles in the pancreas. This is in line with a previously reported role for insulin signaling in promoting vasodilation via nitric-oxide(*105*). Recently, it was established that pericytes can also regulate blood flow in islet capillaries in response to changes in blood glycemic levels(*106*). Therefore, a mechanism whereby pre-capillary arterioles are regulating blood flow along with pericytes through interstitial insulin signaling from β-cells is likely.

Our study has limitations that need to be acknowledged. To relate genes of interest identified in this study to notable biological pathways, we examined the top genes throughout our analysis and then consulted the literature to determine relevant processes. A more comprehensive approach would be to use enrichment analysis with a curated pathway database specific for ECs. However, current databases for gene set and pathway enrichment analysis such as REACTOME, KEGG, Gene Ontology have limited processes involved in vascular functions. Therefore, gene set enrichment using these databases may overlook important biological information present in the data. We also used Harmony to integrate pancreatic EC data from fetal, adult and neonatal datasets. Harmony corrects the principle components obtained from dimensionality reduction techniques. It does not make any changes to the underlying raw count matrix of gene expression values. Therefore, it is not feasible to find DEGs between fetal, neonatal and adult pancreatic EC datasets, as we cannot be sure whether the differences are due to batch effects. However, we can still compare gene expression across different populations found in all three datasets. Developing a normalization or transformation method that removes batch-effects in scRNAseq/snRNAseq gene expression is an ongoing area of intensive research. Finally, we did not conduct *in situ* validation on adult pancreatic tissue. This is because of the high-levels of hydrolytic enzymes in the exocrine pancreas, which we found caused both tissue and RNA probe degradation, as well as autofluorescence, leading to nonspecific background staining that interfered with the accuracy and sensitivity of the staining.

Despite these limitation, we have succeded in tuning out the transcriptomic noise that is inherent in pancreatic endothelial scRNAseq/snRNAseq data and determined a biologically relevant and accurate portrayal of the vascular transcriptomic architecture in the pancreas. Genes of interest and transcriptomic phenomenons highlighted in this study reveal important functional roles of pancreatic ECs in glucose homeostasis and diabetes pathophysiology and also identify important TFs that can aid future endeavours at recapitulating pancreatic islet ECs for regenerative medicine applications.

Materials and Methods

Data Acquisition

Raw counts matrices and meta data for the scRNA-seq/snRNA-seq datasets used in this paper were derived from their respective online databases/repositories. For the Descartes gene expression atlas (https://descartes.brotmanbaty.org/), sparse gene (row) by cell (column) matrices along with cell annotation were downloaded for pancreatic and endothelial cells. For the Tabula Muris gene expression atlas, processed Seurat Robjects for all FACS-sequenced organ datasets were downloaded and the raw count matrices and meta data available for the cells were extracted (https://figshare.com/projects/Tabula_Muris_Transcriptomic_characterization_of_20_organs_and_tissues_from_Mus_musculus_at_single_cell_resolution/27733). Similarly, for the adult and neonatal pancreas data from Tosti et al., processed Seurat Robjects were downloaded (http://singlecell.charite.de/cellbrowser/pancreas/) and the raw count matrices and available meta data were extracted from the objects. For the Tabula Sapiens atlas, processed Seurat Objects

containing all tissue endothelial cell data and pancreas cell data were downloaded and (https://figshare.com/articles/dataset/Tabula_Sapiens_release_1_0/14267219) the raw count matrices and available meta data were pulled from the objects .

Single cell analysis pipeline

Datasets were analyzed using Seurat (v4.0.1). Low quality cells with less than 200 unique genes and genes with 0 counts across all cells were removed. Cells with high unique feature counts (potential doublets or multiplets) above a certain threshold were omitted. The thresholds was determined for each dataset individually based on distribution of feature counts. Cells with high mitochondrial content were filtered out. Data was normalized using log normalization and highly variable genes were detected using variance-stabilizing transformation (vst). The normalized data was centered and scaled and cell cycle scores were generated for each cell using lists of genes expressed in S Phase and G2M Phase. Scoring followed the strategy outlined by Tirosh et at. This data was re-scaled with regression of cell cycle scores and percentage of mitochondrial genes using the vars.to.regress parameter. Dimensionality reduction was performed using the "RunPCA" function, the top 30 principle components were used for non-linear dimension reduction using Uniform Manifold Approximation and Projection (UMAP), with the RunUMAP function. The first 10 principle components were used for Seurat's default graph-based clustering using the FindNeigbhors and FindCluster function.

Differential expression analysis and comparison of differentially expressed genes

Differential expression (DE) analysis was done between cells of interest with the FindMarkers function using the Wilcoxon Rank Sum test. Dissociation induced stress genes (van den Brin, SC, et al. Nat Meth. 2017) were removed from the list. For comparison between mouse genes and human genes, all mouse genes were converted to their human homologues using the R homologene package (1.4.68.19.3.27), for genes that did not have a human homologue, the case of the gene name was converted to capital. For comparisons between genes using different versions of the same gene name, gene lists were updated to their latest approved symbols by comparing to the Hugo Gene Nomenclature Committee (HGNC) database as of April, 2023.

Integrating datasets

To generate the integrated endothelial map, the pancreatic endothelial population from the Descartes fetal pancreas dataset, and the adult and neonatal pancreas dataset from Tosti at al. were merged. The endothelial cell subpopulation from the pancreas datasets were individually processed using the Seurat pipeline detailed above. After clustering, contaminating clusters were identified by comparing differentially expressed genes (DEGs) between clusters. Clusters with differentially upregulated non-vascular markers such as endocrine and exocrine pancreas cell markers were considered contaminating clusters. Once contaminating cells were removed, remaining endothelial cells from the different datasets were merged into one Seurat object using the merge function. The merged object was processed using the Seurat pipeline as detailed above, except the source of the dataset was regressed out while scaling the second time. The data was integrated with Harmony (v1.0) to remove variability from the source of the dataset (Descartes database or from Tosti. et. al.) followed by the individual donor. The resulting integrated or 'harmonized' principal components were used for UMAP dimension reduction and clustering as detailed above.

Scorpius trajectory analysis

Pseudotime trajectory analysis was performed using the R package SCORPIUS. (v1.0.8). Trajectory inference was conducted on UMAP embeddings using the infer_trajectory function. For determining top genes involved in the ordering of the cells along pseudotime, top 50 markers were identified in each cluster in the integrated pancreas EC atlas through DE analysis as described

above. Only the log-normalized counts matrix for these genes were retained to form a truncated expression matrix. SCORPIUS's gene_importances function nwas then matrix was then used to determine genes, whose expression level across the pseudotime best matches the time order using the gene_importances function.

Data visualization

UMAPs, dot plots and volcano plots were generated using SCPubr (v1.1.2)(*107*). Hierchical clustering were generated using ggtree(*108*) (v3.4.4) except for the heatmap for pseudotime trajectory analysis, which was generated using SCORPIUS's draw_trajectory_heatmap function. Venn diagrams were plotted using ggvenn (0.1.9). Scatterplots were generated using ggplot2 (3.4.1). Breaks in violin plots were created using ggbreak (0.1.1)(*109*).

Reference Mapping

To map a query dataset to the reference dataset, anchors were identified using Seurat's FindTransferAnchors function and then the annotations from the reference dataset was projected onto the query using MapQuery

***In situ* immunofluorescence staining**

Tissue cross-sections were obtained from E18.5 mouse pancreatic tissue. Pregnant CD1 dams were euthanized via CO2 asphyxiation, in accordance with IACUC procedures at UT Southwestern Medical Center (UTSW). Embryos were dissected in ice cold -PBS, and pancreata were obtained for fresh-frozen embedding. Pancreata were briefly dabbed on a kimwipe, and washed 1x in Opitimal Cutting Temperature (OCT) media. Pancreata were then placed in OCT-filled embedding and held over liquid nitrogen until frozen. Samples were then stored at -80C. Samples were cryosectioned by UTSW's histology core. Briefly, slides were placed in 4% PFA at room temperature for an hour, and then wash 3X in PBS for 5 minutes per wash. Slides were permebalized with 0.3% Triton for 12 minutes, and then placed in Cas Block (ThermoFisher Cat# 008120). The following primary antibodies were used: Insulin (Cell signaling technology Cat# 4590), Glucagon (Millipore Cat# 4030-01F), VE-Cadherin (Santa Cruz Cat# sc-6458), Pecam1 (Santa Cruz Cat# c-1506), Plvap(BD Pharmingen Cat# 550563). All antibodies were used at a 1:100 dilution, and slides were incubated in primary antibody overnight at 4C. Secondary antibodies conjugated to AlexaFlour were used for visualization.

***In situ* RNAscope™ HiPlex v2 assay**

Tissue cross-sections were obtained from E18.5 mouse pancreatic tissue. Pregnant CD1 dams were euthanized via CO2 asphyxiation, in accordance with IACUC procedures at UT Southwestern Medical Center (UTSW). For RNAscope™ HiPlex v2 assay (Advanced Cell Diagnostics), tissue was processed according to manufacture's instructions. Briefly, slides were fixed in 4% PFA for an hour. Slides were then washed 2x in PBS, and dehydrated to 100% Ethanol. Slides were permeabilized with 12 minutes of protease III treatment. Target probes were applied at 1x concentration, and incubated at 40 degrees for 2 hours. Amplification, fluorophore conjugation, and cleavage was done in accordance with manufacturers protocol. After all probes were imaged, slides were then cleaved 1 more time, washed three times in PBS for 5 minutes per wash. 150 uL of Cas Block was placed in on each slide for 1 hour at room temp, and then primary antibodies were added at a dilution of 1:100. Slides were then incubated in primary antibody overnight at 4°C Secondary antibodies conjugated to AlexaFlour were used for visualization.

***In situ* Visualization**

Images were taken on a nikon a1r confocal, a laser scanning system using the 40x objective (resolution of 3.2 pixels/ 1 μm). For RNA scope images, tile-scan images coupled with zstacks

were taken to obtain large images of the pancreas section. Max Intensity projections were created in ImageJ, and then images were registered using ACD Hiplex Registration software.

***In situ* image quantification**

Images were quantified in a single-blind manner. 10 representative images were taken from the endocrine and exocrine region (based on staining of Insulin/Glucagon) of the capillary vessels based on size. Afterwards these images were analzyed on Fiji by a blinded researcher. RNA Probe channels for *Pecam1* and genes of interest were thresholded using the 'MaxEntropy' option and adjusted accordingly to remove background. Then regions of interest (ROI) was outlined manually based on the Pecam1/Endomucin staining channel. Afterwards, the area of probe was quantified and divided by the area of the ROIs to obtain normalized ratios of RNA probe to area of vessel.

Statistical analysis

Differential expression analysis was conducted using the Wilcoxon Rank Sum Test. Afterwards the p-values obtained were adjusted using the the Bonferroni correction method. For quantification of immunofluorescence staining and RNA probe binding, sample variances were tested for equality using var.equal function in R. If variances were equal then a one-tailed two-sample t-test was conducted, if variances were unequal then a Welch's t-test was conducted.

References

1. S. Rafii, J. M. Butler, B. Sen Ding, Angiocrine functions of organ-specific endothelial cells. *Nature*. **529**, 316 (2016).
2. B. V. Zlokovic, The Blood-Brain Barrier in Health and Chronic Neurodegenerative Disorders. *Neuron*. **57** (2008), pp. 178–201.
3. J. Poisson, S. Lemoinne, C. Boulanger, F. Durand, R. Moreau, D. Valla, P. E. Rautou, Liver sinusoidal endothelial cells: Physiology and role in liver diseases. *J Hepatol*. **66** (2017), pp. 212–227.
4. D. J. Steiner, A. Kim, K. Miller, M. Hara, Pancreatic islet plasticity: Interspecies comparison of islet architecture and composition. *Islets*. **2**, 135 (2010).
5. J. R. Henderson, M. C. Moss, A morphometric study of the endocrine and exocrine capillaries of the pancreas. *Q J Exp Physiol*. **70**, 347–356 (1985).
6. P. Rorsman, F. M. Ashcroft, Pancreatic β-Cell Electrical Activity and Insulin Secretion: Of Mice and Men. *Physiol Rev*. **98**, 117 (2018).
7. L. R. Nyman, E. Ford, A. C. Powers, D. W. Piston, Glucose-dependent blood flow dynamics in murine pancreatic islets in vivo. *Am J Physiol Endocrinol Metab*. **298**, E807 (2010).
8. H. Peiris, C. S. Bonder, P. T. H. Coates, D. J. Keating, C. F. Jessup, The β-cell/EC axis: How do islet cells talk to each other? *Diabetes*. **63** (2014), pp. 3–11.
9. Å. Johansson, J. Lau, M. Sandberg, L. A. H. Borg, P. U. Magnusson, P. O. Carlsson, Endothelial cell signalling supports pancreatic beta cell function in the rat. *Diabetologia*. **52**, 2385–2394 (2009).
10. R. Olsson, P. O. Carlsson, The pancreatic islet endothelial cell: Emerging roles in islet function and disease. *Int J Biochem Cell Biol*. **38**, 710–714 (2006).
11. M. F. Hogan, D. J. Hackney, A. C. Aplin, T. O. Mundinger, M. J. Larmore, J. J. Castillo, N. Esser, S. Zraika, R. L. Hull, SGLT2-i improves markers of islet endothelial cell function in db/db diabetic mice. *J Endocrinol*. **248**, 95–106 (2021).

677 12. J. C. Schupp, T. S. Adams, C. Cosme, M. S. B. Raredon, Y. Yuan, N. Omote, S. Poli, M.
678 Chioccioli, K. A. Rose, E. P. Manning, M. Sauler, G. Deiuliis, F. Ahangari, N. Neumark,
679 A. C. Habermann, A. J. Gutierrez, L. T. Bui, R. Lafyatis, R. W. Pierce, K. B. Meyer, M.
680 C. Nawijn, S. A. Teichmann, N. E. Banovich, J. A. Kropski, L. E. Niklason, D. Pe'er, X.
681 Yan, R. J. Homer, I. O. Rosas, N. Kaminski, Integrated Single-Cell Atlas of Endothelial
682 Cells of the Human Lung. *Circulation* (2021),
683 doi:10.1161/CIRCULATIONAHA.120.052318.
684 13. A. C. Yang, R. T. Vest, F. Kern, D. P. Lee, M. Agam, C. A. Maat, P. M. Losada, M. B.
685 Chen, N. Schaum, N. Khoury, A. Toland, K. Calcuttawala, H. Shin, R. Pálovics, A. Shin,
686 E. Y. Wang, J. Luo, D. Gate, W. J. Schulz-Schaeffer, P. Chu, J. A. Siegenthaler, M. W.
687 McNerney, A. Keller, T. Wyss-Coray, A human brain vascular atlas reveals diverse
688 mediators of Alzheimer's risk. *Nature*. **603**, 885 (2022).
689 14. M. Enge, H. E. Arda, M. Mignardi, J. Beausang, R. Bottino, S. K. Kim, S. R. Quake,
690 Single-Cell Analysis of Human Pancreas Reveals Transcriptional Signatures of Aging and
691 Somatic Mutation Patterns. *Cell*. **171**, 321 (2017).
692 15. J. Camunas-Soler, X. Q. Dai, Y. Hang, A. Bautista, J. Lyon, K. Suzuki, S. K. Kim, S. R.
693 Quake, P. E. MacDonald, Patch-seq links single-cell transcriptomes to human islet
694 dysfunction in diabetes. *Cell Metab*. **31**, 1017 (2020).
695 16. N. Lawlor, J. George, M. Bolisetty, R. Kursawe, L. Sun, V. Sivakamasundari, I. Kycia, P.
696 Robson, M. L. Stitzel, Single-cell transcriptomes identify human islet cell signatures and
697 reveal cell-type-specific expression changes in type 2 diabetes. *Genome Res*. **27**, 208–222
698 (2017).
699 17. M. Baron, A. Veres, S. L. Wolock, A. L. Faust, R. Gaujoux, A. Vetere, J. H. Ryu, B. K.
700 Wagner, S. S. Shen-Orr, A. M. Klein, D. A. Melton, I. Yanai, A Single-Cell
701 Transcriptomic Map of the Human and Mouse Pancreas Reveals Inter- and Intra-cell
702 Population Structure. *Cell Syst*. **3**, 346-360.e4 (2016).
703 18. M. J. Muraro, G. Dharmadhikari, D. Grün, N. Groen, T. Dielen, E. Jansen, L. van Gurp,
704 M. A. Engelse, F. Carlotti, E. J. P. de Koning, A. van Oudenaarden, A Single-Cell
705 Transcriptome Atlas of the Human Pancreas. *Cell Syst*. **3**, 385 (2016).
706 19. Å. Segerstolpe, A. Palasantza, P. Eliasson, E. M. Andersson, A. C. Andréasson, X. Sun, S.
707 Picelli, A. Sabirsh, M. Clausen, M. K. Bjursell, D. M. Smith, M. Kasper, C. Ämmälä, R.
708 Sandberg, Single-Cell Transcriptome Profiling of Human Pancreatic Islets in Health and
709 Type 2 Diabetes. *Cell Metab*. **24**, 593–607 (2016).
710 20. D. Nyqvist, M. Köhler, H. Wahlstedt, P. O. Berggren, Donor Islet Endothelial Cells
711 Participate in Formation of Functional Vessels Within Pancreatic Islet Grafts. *Diabetes*.
712 **54**, 2287–2293 (2005).
713 21. B. Vieth, S. Parekh, C. Ziegenhain, W. Enard, I. Hellmann, A systematic evaluation of
714 single cell RNA-seq analysis pipelines. *Nat Commun*. **10** (2019), doi:10.1038/S41467-
715 019-12266-7.
716 22. J. Kalucka, L. P. M. H. de Rooij, J. Goveia, K. Rohlenova, S. J. Dumas, E. Meta, N. V.
717 Conchinha, F. Taverna, L. A. Teuwen, K. Veys, M. García-Caballero, S. Khan, V.
718 Geldhof, L. Sokol, R. Chen, L. Treps, M. Borri, P. de Zeeuw, C. Dubois, T. K. Karakach,
719 K. D. Falkenberg, M. Parys, X. Yin, S. Vinckier, Y. Du, R. A. Fenton, L. Schoonjans, M.
720 Dewerchin, G. Eelen, B. Thienpont, L. Lin, L. Bolund, X. Li, Y. Luo, P. Carmeliet,
721 Single-Cell Transcriptome Atlas of Murine Endothelial Cells. *Cell*. **180**, 764-779.e20
722 (2020).

723 23. D. T. Paik, L. Tian, I. M. Williams, S. Rhee, H. Zhang, C. Liu, R. Mishra, S. M. Wu, K.
724 Red-Horse, J. C. Wu, Single-Cell RNA-seq Unveils Unique Transcriptomic Signatures of
725 Organ-Specific Endothelial Cells. *Circulation* (2020),
726 doi:10.1161/circulationaha.119.041433.
727 24. W. Feng, L. Chen, P. K. Nguyen, S. M. Wu, G. Li, Single Cell Analysis of Endothelial
728 Cells Identified Organ-Specific Molecular Signatures and Heart-Specific Cell Populations
729 and Molecular Features. *Front Cardiovasc Med*. **6**, 165 (2019).
730 25. N. Schaum, J. Karkanias, N. F. Neff, A. P. May, S. R. Quake, T. Wyss-Coray, S.
731 Darmanis, J. Batson, O. Botvinnik, M. B. Chen, S. Chen, F. Green, R. C. Jones, A.
732 Maynard, L. Penland, A. O. Pisco, R. V. Sit, G. M. Stanley, J. T. Webber, F. Zanini, A. S.
733 Baghel, I. Bakerman, I. Bansal, D. Berdnik, B. Bilen, D. Brownfield, C. Cain, M. Cho, G.
734 Cirolia, S. D. Conley, A. Demers, K. Demir, A. de Morree, T. Divita, H. du Bois, L. B. T.
735 Dulgeroff, H. Ebadi, F. H. Espinoza, M. Fish, Q. Gan, B. M. George, A. Gillich, G.
736 Genetiano, X. Gu, G. S. Gulati, Y. Hang, S. Hosseinzadeh, A. Huang, T. Iram, T. Isobe, F.
737 Ives, K. S. Kao, G. Karnam, A. M. Kershner, B. M. Kiss, W. Kong, M. E. Kumar, J. Y.
738 Lam, D. P. Lee, S. E. Lee, G. Li, Q. Li, L. Liu, A. Lo, W. J. Lu, A. Manjunath, K. L. May,
739 O. L. May, M. McKay, R. J. Metzger, M. Mignardi, D. Min, A. N. Nabhan, K. M. Ng, J.
740 Noh, R. Patkar, W. C. Peng, R. Puccinelli, E. J. Rulifson, S. S. Sikandar, R. Sinha, K.
741 Szade, W. Tan, C. Tato, K. Tellez, K. J. Travaglini, C. Tropini, L. Waldburger, L. J. van
742 Weele, M. N. Wosczyna, J. Xiang, S. Xue, J. Youngyunpipatkul, M. E. Zardeneta, F.
743 Zhang, L. Zhou, P. Castro, D. Croote, J. L. DeRisi, C. S. Kuo, B. Lehallier, P. K. Nguyen,
744 S. Y. Tan, B. M. Wang, H. Yousef, P. A. Beachy, C. K. F. Chan, K. C. Huang, K.
745 Weinberg, S. M. Wu, B. A. Barres, M. F. Clarke, S. K. Kim, M. A. Krasnow, R. Nusse, T.
746 A. Rando, J. Sonnenburg, I. L. Weissman, Single-cell transcriptomics of 20 mouse organs
747 creates a Tabula Muris. *Nature*. **562**, 367–372 (2018).
748 26. J. Cao, D. R. O'Day, H. A. Pliner, P. D. Kingsley, M. Deng, R. M. Daza, M. A. Zager, K.
749 A. Aldinger, R. Blecher-Gonen, F. Zhang, M. Spielmann, J. Palis, D. Doherty, F. J.
750 Steemers, I. A. Glass, C. Trapnell, J. Shendure, A human cell atlas of fetal gene
751 expression. *Science (1979)*. **370** (2020),
752 doi:10.1126/SCIENCE.ABA7721/SUPPL_FILE/ABA7721_TABLESS1-S16.XLSX.
753 27. R. C. Jones, J. Karkanias, M. A. Krasnow, A. O. Pisco, S. R. Quake, J. Salzman, N.
754 Yosef, B. Bulthaup, P. Brown, W. Harper, M. Hemenez, R. Ponnusamy, A. Salehi, B. A.
755 Sanagavarapu, E. Spallino, K. A. Aaron, W. Concepcion, J. M. Gardner, B. Kelly, N.
756 Neidlinger, Z. Wang, S. Crasta, S. Kolluru, M. Morri, A. O. Pisco, S. Y. Tan, K. J.
757 Travaglini, C. Xu, M. Alcántara-Hernández, N. Almanzar, J. Antony, B. Beyersdorf, D.
758 Burhan, K. Calcuttawala, M. M. Carter, C. K. F. Chan, C. A. Chang, S. Chang, A.
759 Colville, S. Crasta, R. N. Culver, I. Cvijović, G. D'Amato, C. Ezran, F. X. Galdos, A.
760 Gillich, W. R. Goodyer, Y. Hang, A. Hayashi, S. Houshdaran, X. Huang, J. C. Irwin, S.
761 Jang, J. V. Juanico, A. M. Kershner, S. Kim, B. Kiss, S. Kolluru, W. Kong, M. E. Kumar,
762 A. H. Kuo, R. Leylek, B. Li, G. B. Loeb, W.-J. Lu, S. Mantri, M. Markovic, P. L.
763 McAlpine, A. de Morree, M. Morri, K. Mrouj, S. Mukherjee, T. Muser, P. Neuhöfer, T. D.
764 Nguyen, K. Perez, R. Phansalkar, A. O. Pisco, N. Puluca, Z. Qi, P. Rao, H. Raquer-
765 McKay, N. Schaum, B. Scott, B. Seddighzadeh, J. Segal, S. Sen, S. Sikandar, S. P.
766 Spencer, L. C. Steffes, V. R. Subramaniam, A. Swarup, M. Swift, K. J. Travaglini, W.
767 Van Treuren, E. Trimm, S. Veizades, S. Vijayakumar, K. C. Vo, S. K. Vorperian, W.
768 Wang, H. N. W. Weinstein, J. Winkler, T. T. H. Wu, J. Xie, A. R. Yung, Y. Zhang, A. M.
769 Detweiler, H. Mekonen, N. F. Neff, R. V. Sit, M. Tan, J. Yan, G. R. Bean, V. Charu, E.

770 Forgó, B. A. Martin, M. G. Ozawa, O. Silva, S. Y. Tan, A. Toland, V. N. P. Vemuri, S.
771 Afik, K. Awayan, O. B. Botvinnik, A. Byrne, M. Chen, R. Dehghannasiri, A. M.
772 Detweiler, A. Gayoso, A. A. Granados, Q. Li, G. Mahmoudabadi, A. McGeever, A. de
773 Morree, J. E. Olivieri, M. Park, A. O. Pisco, N. Ravikumar, J. Salzman, G. Stanley, M.
774 Swift, M. Tan, W. Tan, A. J. Tarashansky, R. Vanheusden, S. K. Vorperian, P. Wang, S.
775 Wang, G. Xing, C. Xu, N. Yosef, M. Alcántara-Hernández, J. Antony, C. K. F. Chan, C.
776 A. Chang, A. Colville, S. Crasta, R. Culver, L. Dethlefsen, C. Ezran, A. Gillich, Y. Hang,
777 P.-Y. Ho, J. C. Irwin, S. Jang, A. M. Kershner, W. Kong, M. E. Kumar, A. H. Kuo, R.
778 Leylek, S. Liu, G. B. Loeb, W.-J. Lu, J. S. Maltzman, R. J. Metzger, A. de Morree, P.
779 Neuhöfer, K. Perez, R. Phansalkar, Z. Qi, P. Rao, H. Raquer-McKay, K. Sasagawa, B.
780 Scott, R. Sinha, H. Song, S. P. Spencer, A. Swarup, M. Swift, K. J. Travaglini, E. Trimm,
781 S. Veizades, S. Vijayakumar, B. Wang, W. Wang, J. Winkler, J. Xie, A. R. Yung, S. E.
782 Artandi, P. A. Beachy, M. F. Clarke, L. C. Giudice, F. W. Huang, K. C. Huang, J.
783 Idoyaga, S. K. Kim, M. Krasnow, C. S. Kuo, P. Nguyen, S. R. Quake, T. A. Rando, K.
784 Red-Horse, J. Reiter, D. A. Relman, J. L. Sonnenburg, B. Wang, A. Wu, S. M. Wu, T.
785 Wyss-Coray, The Tabula Sapiens: A multiple-organ, single-cell transcriptomic atlas of
786 humans. *Science (1979)*. **376** (2022),
787 doi:10.1126/SCIENCE.ABL4896/SUPPL_FILE/SCIENCE.ABL4896_MDAR_REPROD
788 UCIBILITY_CHECKLIST.PDF.
789 28. B. Marquina-Sanchez, N. Fortelny, M. Farlik, A. Vieira, P. Collombat, C. Bock, S.
790 Kubicek, Single-cell RNA-seq with spike-in cells enables accurate quantification of cell-
791 specific drug effects in pancreatic islets. *Genome Biol*. **21** (2020), doi:10.1186/S13059-
792 020-02006-2.
793 29. M. D. Young, S. Behjati, SoupX removes ambient RNA contamination from droplet-
794 based single-cell RNA sequencing data. *Gigascience*. **9**, 1–10 (2020).
795 30. S. Yang, S. E. Corbett, Y. Koga, Z. Wang, W. E. Johnson, M. Yajima, J. D. Campbell,
796 Decontamination of ambient RNA in single-cell RNA-seq with DecontX. *Genome Biol*.
797 **21** (2020), doi:10.1186/S13059-020-1950-6.
798 31. L. Tosti, Y. Hang, O. Debnath, S. Tiesmeyer, T. Trefzer, K. Steiger, F. W. Ten, S.
799 Lukassen, S. Ballke, A. A. Kühl, S. Spieckermann, R. Bottino, N. Ishaque, W. Weichert,
800 S. K. Kim, R. Eils, C. Conrad, Single-Nucleus and In Situ RNA–Sequencing Reveal Cell
801 Topographies in the Human Pancreas. *Gastroenterology*. **160**, 1330-1344.e11 (2021).
802 32. Y. Hao, S. Hao, E. Andersen-Nissen, W. M. Mauck, S. Zheng, A. Butler, M. J. Lee, A. J.
803 Wilk, C. Darby, M. Zager, P. Hoffman, M. Stoeckius, E. Papalexi, E. P. Mimitou, J. Jain,
804 A. Srivastava, T. Stuart, L. M. Fleming, B. Yeung, A. J. Rogers, J. M. McElrath, C. A.
805 Blish, R. Gottardo, P. Smibert, R. Satija, Integrated analysis of multimodal single-cell
806 data. *Cell*. **184**, 3573 (2021).
807 33. I. Tirosh, B. Izar, S. M. Prakadan, M. H. Wadsworth, D. Treacy, J. J. Trombetta, A.
808 Rotem, C. Rodman, C. Lian, G. Murphy, M. Fallahi-Sichani, K. Dutton-Regester, J. R.
809 Lin, O. Cohen, P. Shah, D. Lu, A. S. Genshaft, T. K. Hughes, C. G. K. Ziegler, S. W.
810 Kazer, A. Gaillard, K. E. Kolb, A. C. Villani, C. M. Johannessen, A. Y. Andreev, E. M.
811 Van Allen, M. Bertagnolli, P. K. Sorger, R. J. Sullivan, K. T. Flaherty, D. T. Frederick, J.
812 Jané-Valbuena, C. H. Yoon, O. Rozenblatt-Rosen, A. K. Shalek, A. Regev, L. A.
813 Garraway, Dissecting the multicellular ecosystem of metastatic melanoma by single-cell
814 RNA-seq. *Science*. **352**, 189 (2016).
815 34. W. Yu, J. P. Hegarty, A. Berg, X. Chen, G. West, A. A. Kelly, Y. Wang, L. S. Poritz, W.
816 A. Koltun, Z. Lin, NKX2-3 Transcriptional Regulation of Endothelin-1 and VEGF

817 Signaling in Human Intestinal Microvascular Endothelial Cells. *PLoS One*. **6**, e20454
818 (2011).
819 35. P. M. Fernandez-Salguero, J. M. Ward, J. P. Sundberg, F. J. Gonzalez, Lesions of Aryl-
820 hydrocarbon Receptor–deficient Mice. *http://dx.doi.org/10.1177/030098589703400609*.
821 **34**, 605–614 (1997).
822 36. S. Ichihara, Y. Yamada, G. Ichihara, T. Nakajima, P. Li, T. Kondo, F. J. Gonzalez, T.
823 Murohara, A role for the aryl hydrocarbon receptor in regulation of ischemia-induced
824 angiogenesis. *Arterioscler Thromb Vasc Biol*. **27**, 1297–1304 (2007).
825 37. H. C. Wang, T. H. Wong, L. T. Wang, H. H. Su, H. Y. Yu, A. H. Wu, Y. C. Lin, H. L.
826 Chen, J. L. Suen, S. H. Hsu, L. C. Chen, Y. Zhou, S. K. Huang, Aryl hydrocarbon receptor
827 signaling promotes ORMDL3-dependent generation of sphingosine-1-phosphate by
828 inhibiting sphingosine-1-phosphate lyase. *Cell Mol Immunol*. **16**, 783 (2019).
829 38. J. C. Stanford, A. J. Morris, M. Sunkara, G. J. Popa, K. L. Larson, S. Özcan, Sphingosine
830 1-Phosphate (S1P) Regulates Glucose-stimulated Insulin Secretion in Pancreatic Beta
831 Cells. *J Biol Chem*. **287**, 13457 (2012).
832 39. H. Shimizu, F. Okajima, T. Kimura, K. I. Ohtani, T. Tsuchiya, H. Takahashi, A.
833 Kuwabara, H. Tomura, K. Sato, M. Mori, Sphingosine 1-phosphate stimulates insulin
834 secretion in HIT-T 15 cells and mouse islets. *Endocr J*. **47**, 261–269 (2000).
835 40. D. M. Adyshev, N. K. Moldobaeva, V. R. Elangovan, J. G. N. Garcia, S. M. Dudek,
836 Differential involvement of ezrin/radixin/moesin proteins in sphingosine 1-phosphate-
837 induced human pulmonary endothelial cell barrier enhancement. *Cell Signal*. **23**, 2086
838 (2011).
839 41. H. Goto, M. Miyamoto, A. Kihara, Direct uptake of sphingosine-1-phosphate independent
840 of phospholipid phosphatases. *Journal of Biological Chemistry*. **296**, 100605 (2021).
841 42. I. Usui, T. Imamura, J. Huang, H. Satoh, J. M. Olefsky, Cdc42 Is a Rho TGPase family
842 member that can mediate insulin signaling to glucose transport in 3T3-L1 adipocytes.
843 *Journal of Biological Chemistry*. **278**, 13765–13774 (2003).
844 43. L. Q. Dong, L. R. Landa, M. J. Wick, L. Zhu, H. Mukai, Y. Ono, F. Liu, Phosphorylation
845 of protein kinase N by phosphoinositide-dependent protein kinase-1 mediates insulin
846 signals to the actin cytoskeleton. *Proc Natl Acad Sci U S A*. **97**, 5089 (2000).
847 44. M. Standaert, G. Bandyopadhyay, L. Galloway, Y. Ono, H. Mukai, R. Farese,
848 Comparative Effects of GTPγS and Insulin on the Activation of Rho, Phosphatidylinositol
849 3-Kinase, and Protein Kinase N in Rat Adipocytes: RELATIONSHIP TO GLUCOSE
850 TRANSPORT *. *Journal of Biological Chemistry*. **273**, 7470–7477 (1998).
851 45. B. J. de Kreuk, A. R. Gingras, J. D. R. Knight, J. J. Liu, A. C. Gingras, M. H. Ginsberg,
852 Heart of glass anchors Rasip1 at endothelial cell-cell junctions to support vascular
853 integrity. *Elife*. **5** (2016), doi:10.7554/ELIFE.11394.
854 46. S. Ioannidou, K. Deinhardt, J. Miotla, J. Bradley, E. Cheung, S. Samuelsson, Y. S. Ng, D.
855 T. Shima, From the Cover: An in vitro assay reveals a role for the diaphragm protein PV-1
856 in endothelial fenestra morphogenesis. *Proc Natl Acad Sci U S A*. **103**, 16770 (2006).
857 47. S. S. Rho, H. J. Choi, J. K. Min, H. W. Lee, H. Park, H. Park, Y. M. Kim, Y. G. Kwon,
858 Clec14a is specifically expressed in endothelial cells and mediates cell to cell adhesion.
859 *Biochem Biophys Res Commun*. **404**, 103–108 (2011).
860 48. T. S. Adams, J. C. Schupp, S. Poli, E. A. Ayaub, N. Neumark, F. Ahangari, S. G. Chu, B.
861 A. Raby, G. DeIuliis, M. Januszyk, Q. Duan, H. A. Arnett, A. Siddiqui, G. R. Washko, R.
862 Homer, X. Yan, I. O. Rosas, N. Kaminski, Single-cell RNA-seq reveals ectopic and

863 aberrant lung-resident cell populations in idiopathic pulmonary fibrosis. *Sci Adv*. **6** (2020),
864 doi:10.1126/SCIADV.ABA1983.
865 49. E. V. Quadros, J. M. Sequeira, Cellular Uptake of Cobalamin: Transcobalamin and the
866 TCblR/CD320 Receptor. *Biochimie*. **95**, 1008 (2013).
867 50. N. Kanai, R. Lu, J. A. Satriano, Y. Bao, A. W. Wolkoff, V. L. Schuster, Identification and
868 characterization of a prostaglandin transporter. *Science*. **268**, 866–869 (1995).
869 51. N. J. Palpant, L. Pabon, J. S. Rabinowitz, B. K. Hadland, C. L. Stoick-Cooper, S. L. Paige,
870 I. D. Bernstein, R. T. Moon, C. E. Murry, Transmembrane protein 88: A Wnt regulatory
871 protein that specifies cardiomyocyte development. *Development (Cambridge)*. **140**, 3799–
872 3808 (2013).
873 52. S. Y. Park, X. Shi, J. Pang, C. Yan, B. C. Berk, Thioredoxin-Interacting Protein Mediates
874 Sustained VEGFR2 Signaling in Endothelial Cells required for Angiogenesis. *Arterioscler*
875 *Thromb Vasc Biol*. **33**, 737 (2013).
876 53. J. P. Girard, T. A. Springer, Cloning from purified high endothelial venule cells of hevin,
877 a close relative of the antiadhesive extracellular matrix protein SPARC. *Immunity*. **2**, 113–
878 123 (1995).
879 54. E. Naschberger, A. Liebl, V. S. Schellerer, M. Schütz, N. Britzen-Laurent, P. Klbel, U.
880 Schaal, L. Haep, D. Regensburger, T. Wittmann, L. Klein-Hitpass, T. T. Rau, B. Dietel,
881 V. S. Méniel, A. R. Clarke, S. Merke, R. S. Croner, W. Hohenberger, M. Stürzl,
882 Matricellular protein SPARCL1 regulates tumor microenvironment–dependent endothelial
883 cell heterogeneity in colorectal carcinoma. *J Clin Invest*. **126**, 4187–4204 (2016).
884 55. M. Tichet, V. Prodhomme, N. Fenouille, D. Ambrosetti, A. Mallavialle, M. Cerezo, M.
885 Ohanna, S. Audebert, S. Rocchi, D. Giacchero, F. Boukari, M. Allegra, J. C. Chambard, J.
886 P. Lacour, J. F. Michiels, J. P. Borg, M. Deckert, S. Tartare-Deckert, Tumour-derived
887 SPARC drives vascular permeability and extravasation through endothelial VCAM1
888 signalling to promote metastasis. *Nature Communications 2015 6:1*. **6**, 1–15 (2015).
889 56. C. Atorrasagasti, A. Onorato, M. L. Gimeno, L. Andreone, M. Garcia, M. Malvicini, E.
890 Fiore, J. Bayo, M. J. Perone, G. D. Mazzolini, SPARC is required for the maintenance of
891 glucose homeostasis and insulin secretion in mice. *Clin Sci (Lond)*. **133**, 351–365 (2019).
892 57. M. Downes, P. Koopman, SOX18 and the Transcriptional Regulation of Blood Vessel
893 Development. *Trends Cardiovasc Med*. **11**, 318–324 (2001).
894 58. G. Ferrari, B. D. Cook, V. Terushkin, G. Pintucci, P. Mignatti, TRANSFORMING
895 GROWTH FACTOR-BETA 1 (TGF-β1) INDUCES ANGIOGENESIS THROUGH
896 VASCULAR ENDOTHELIAL GROWTH FACTOR (VEGF)-MEDIATED
897 APOPTOSIS. *J Cell Physiol*. **219**, 449 (2009).
898 59. R. B. Reinert, Q. Cai, J. Y. Hong, J. L. Plank, K. Aamodt, N. Prasad, R. Aramandla, C.
899 Dai, S. E. Levy, A. Pozzi, P. A. Labosky, C. V. E. Wright, M. Brissova, A. C. Powers,
900 Vascular endothelial growth factor coordinates islet innervation via vascular scaffolding.
901 *Development (Cambridge)*. **141**, 1480–1491 (2014).
902 60. Y. S. Kim, S. H. Jung, D. H. Jung, S. J. Choi, Y. R. Lee, J. S. Kim, Gas6 Stimulates
903 Angiogenesis of Human Retinal Endothelial Cells and of Zebrafish Embryos via ERK1/2
904 Signaling. *PLoS One*. **9**, e83901 (2014).
905 61. Y. Jiang, J. Huang, Y. Xia, Z. Sun, P. Hu, D. Wang, Y. Liu, T. Tao, Y. Liu, Hypoxia
906 activates GPR146 which participates in pulmonary vascular remodeling by promoting
907 pyroptosis of pulmonary artery endothelial cells. *Eur J Pharmacol*. **941**, 175502 (2023).
908 62. F. Hall-Glenn, R. A. de Young, B. L. Huang, B. van Handel, J. J. Hofmann, T. T. Chen,
909 A. Choi, J. R. Ong, P. D. Benya, H. Mikkola, M. L. Iruela-Arispe, K. M. Lyons,

910 CCN2/Connective Tissue Growth Factor Is Essential for Pericyte Adhesion and
911 Endothelial Basement Membrane Formation during Angiogenesis. *PLoS One*. **7**, e30562
912 (2012).
913 63. S. M. Wasserman, F. Mehraban, L. G. Komuves, R. B. Yang, J. E. Tomlinson, Y. Zhang,
914 F. Spriggs, J. N. Topper, Gene expression profile of human endothelial cells exposed to
915 sustained fluid shear stress. *Physiol Genomics*. **12**, 13–23 (2002).
916 64. F. C. Lynn, L. Sanchez, R. Gomis, M. S. German, R. Gasa, Identification of the bHLH
917 Factor Math6 as a Novel Component of the Embryonic Pancreas Transcriptional Network.
918 *PLoS One*. **3**, e2430 (2008).
919 65. I. Korsunsky, N. Millard, J. Fan, K. Slowikowski, F. Zhang, K. Wei, Y. Baglaenko, M.
920 Brenner, P. ru Loh, S. Raychaudhuri, Fast, sensitive and accurate integration of single-cell
921 data with Harmony. *Nat Methods*. **16**, 1289–1296 (2019).
922 66. I. Buschmann, A. Pries, B. Styp-Rekowska, P. Hillmeister, L. Loufrani, D. Henrion, Y.
923 Shi, A. Duelsner, I. Hoefer, N. Gatzke, H. Wang, K. Lehmann, L. Ulm, Z. Ritter, P.
924 Hauff, R. Hlushchuk, V. Djonov, T. Van Veen, F. Le Noble, Pulsatile shear and Gja5
925 modulate arterial identity and remodeling events during flow-driven arteriogenesis.
926 *Development*. **137**, 2187–2196 (2010).
927 67. J. S. Fang, B. G. Coon, N. Gillis, Z. Chen, J. Qiu, T. W. Chittenden, J. M. Burt, M. A.
928 Schwartz, K. K. Hirschi, Shear-induced Notch-Cx37-p27 axis arrests endothelial cell
929 cycle to enable arterial specification. *Nature Communications 2017 8:1*. **8**, 1–14 (2017).
930 68. D. Shin, G. Garcia-Cardena, S. I. Hayashi, S. Gerety, T. Asahara, G. Stavrakis, J. Isner, J.
931 Folkman, M. A. Gimbrone, D. J. Anderson, Expression of ephrinB2 identifies a stable
932 genetic difference between arterial and venous vascular smooth muscle as well as
933 endothelial cells, and marks subsets of microvessels at sites of adult neovascularization.
934 *Dev Biol*. **230**, 139–150 (2001).
935 69. B. Gorsi, F. Liu, X. Ma, T. J. A. Chico, A. Shrinivasan, K. L. Kramer, E. Bridges, R.
936 Monteiro, A. L. Harris, R. Patient, S. E. Stringer, The heparan sulfate editing enzyme
937 Sulf1 plays a novel role in zebrafish VegfA mediated arterial venous identity.
938 *Angiogenesis*. **17**, 77–91 (2014).
939 70. A. Thiriot, C. Perdomo, G. Cheng, I. Novitzky-Basso, S. McArdle, J. K. Kishimoto, O.
940 Barreiro, I. Mazo, R. Triboulet, K. Ley, A. Rot, U. H. von Andrian, Differential
941 DARC/ACKR1 expression distinguishes venular from non-venular endothelial cells in
942 murine tissues. *BMC Biol*. **15**, 1–19 (2017).
943 71. R. V. Stan, M. Kubitza, G. E. Palade, PV-1 is a component of the fenestral and stomatal
944 diaphragms in fenestrated endothelia. *Proc Natl Acad Sci U S A*. **96**, 13203 (1999).
945 72. C. G. Hansen, N. A. Bright, G. Howard, B. J. Nichols, SDPR induces membrane curvature
946 and functions in the formation of caveolae. *Nature Cell Biology 2009 11:7*. **11**, 807–814
947 (2009).
948 73. I. Yeow, G. Howard, J. Chadwick, C. Mendoza-Topaz, C. G. Hansen, B. J. Nichols, E.
949 Shvets, EHD Proteins Cooperate to Generate Caveolar Clusters and to Maintain Caveolae
950 during Repeated Mechanical Stress. *Current Biology*. **27**, 2951 (2017).
951 74. N. Gil-Yarom, L. Radomir, L. Sever, M. P. Kramer, H. Lewinsky, C. Bornstein, R.
952 Blecher-Gonen, Z. Barnett-Itzhaki, V. Mirkin, G. Friedlander, L. Shvidel, Y. Herishanu,
953 E. J. Lolis, S. Becker-Herman, I. Amit, I. Shachar, CD74 is a novel transcription regulator.
954 *Proc Natl Acad Sci U S A*. **114**, 562 (2017).

955 75. S. M. Moore, V. V. Holt, L. R. Malpass, I. N. Hines, M. D. Wheeler, Fatty acid-binding
956 protein 5 limits the anti-inflammatory response in murine macrophages. *Mol Immunol*. **67**,
957 265 (2015).
958 76. R. Alejandro, F. L. Shienvold, S. Vaerewyck Hajek, U. Ryan, J. Miller, D. H. Mintz,
959 Immunocytochemical Localization of HLA-DR in Human Islets of Langerhans. *Diabetes*.
960 **31**, 17–22 (1982).
961 77. D. Van Breevoort, E. L. Van Agtmaal, B. S. Dragt, J. K. Gebbinck, I. Dienava-Verdoold,
962 A. Kragt, R. Bierings, A. J. G. Horrevoets, K. M. Valentijn, J. C. Eikenboom, M.
963 Fernandez-Borja, A. B. Meijer, J. Voorberg, Proteomic screen identifies IGFBP7 as a
964 novel component of endothelial cell-specific Weibel-Palade bodies. *J Proteome Res*. **11**,
965 2925–2936 (2012).
966 78. E. Komiya, H. Sato, N. Watanabe, M. Ise, S. Higashi, Y. Miyagi, K. Miyazaki,
967 Angiomodulin, a marker of cancer vasculature, is upregulated by vascular endothelial
968 growth factor and increases vascular permeability as a ligand of integrin αvβ3. *Cancer*
969 *Med*. **3**, 537 (2014).
970 79. Y. Zhou, J. Williams, P. M. Smallwood, J. Nathans, Sox7, Sox17, and Sox18
971 Cooperatively Regulate Vascular Development in the Mouse Retina. *PLoS One*. **10**,
972 e0143650 (2015).
973 80. W. Saelens, R. Cannoodt, H. Todorov, Y. Saeys, A comparison of single-cell trajectory
974 inference methods. *Nat Biotechnol*. **37**, 547–554 (2019).
975 81. K. Boyé, L. H. Geraldo, J. Furtado, L. Pibouin-Fragner, M. Poulet, D. Kim, B. Nelson, Y.
976 Xu, L. Jacob, N. Maissa, D. Agalliu, L. Claesson-Welsh, S. L. Ackerman, A. Eichmann,
977 Endothelial Unc5B controls blood-brain barrier integrity. *Nature Communications 2022*
978 *13:1*. **13**, 1–15 (2022).
979 82. Y. Aghazadeh, S. T. Khan, B. Nkennor, S. S. Nunes, Cell-based therapies for vascular
980 regeneration: Past, present and future. *Pharmacol Ther*. **231**, 107976 (2022).
981 83. Y. Aghazadeh, S. T. Khan, B. Nkennor, S. S. Nunes, Cell-based therapies for vascular
982 regeneration: Past, present and future. *Pharmacol Ther*, 107976 (2021).
983 84. S. S. Hasan, M. Jabs, J. Taylor, L. Wiedmann, T. Leibing, V. Nordström, G. Federico, L.
984 P. Roma, C. Carlein, G. Wolff, B. Ekim-Üstünel, M. Brune, I. Moll, F. Tetzlaff, H.-J.
985 Gröne, T. Fleming, C. Géraud, S. Herzig, P. P. Nawroth, A. Fischer, Endothelial Notch
986 signaling controls insulin transport in muscle. *EMBO Mol Med*. **12**, e09271 (2020).
987 85. J. Gustavsson, S. Parpal, P. Strålfors, Insulin-stimulated glucose uptake involves the
988 transition of glucose transporters to a caveolae-rich fraction within the plasma membrane:
989 Implications for type II diabetes. *Molecular Medicine*. **2**, 367–372 (1996).
990 86. H. Wang, A. X. Wang, E. J. Barrett, Caveolin-1 is required for vascular endothelial insulin
991 uptake. *Am J Physiol Endocrinol Metab*. **300**, E134 (2011).
992 87. S. Hayashi, M. P. Scott, What determines the specificity of action of Drosophila
993 homeodomain proteins? *Cell*. **63**, 883–894 (1990).
994 88. M. N. Stanfel, K. A. Moses, R. J. Schwartz, W. E. Zimmer, Regulation of organ
995 development by the NKX-homeodomain factors: an NKX code. *Cell Mol Biol (Noisy-le-*
996 *grand)*. **Suppl 51**, OL785-99 (2005).
997 89. O. Pabst, R. Zweigerdt, H. H. Arnold, Targeted disruption of the homeobox transcription
998 factor Nkx2-3 in mice results in postnatal lethality and abnormal development of small
999 intestine and spleen. *Development*. **126**, 2215–2225 (1999).

1000 90. T. Czömpöly, Á. Lábadi, Z. Kellermayer, K. Olasz, H.-H. Arnold, P. Balogh,
1001 Transcription Factor Nkx2-3 Controls the Vascular Identity and Lymphocyte Homing in
1002 the Spleen. *The Journal of Immunology*. **186**, 6981–6989 (2011).
1003 91. T. T. Dinh, M. Xiang, A. Rajaraman, Y. Wang, N. Salazar, Y. Zhu, W. Roper, S. Rhee, K.
1004 Brulois, E. O'Hara, H. Kiefel, T. M. Dinh, Y. Bi, D. Gonzalez, E. P. Bao, K. Red-Horse,
1005 P. Balogh, F. Gábris, B. Gaszner, G. Berta, J. Pan, E. C. Butcher, An NKX-COUP-TFII
1006 morphogenetic code directs mucosal endothelial addressin expression. *Nature*
1007 *Communications 2022 13:1*. **13**, 1–14 (2022).
1008 92. C. C. Wang, C. Biben, L. Robb, F. Nassir, L. Barnett, N. O. Davidson, F. Koentgen, D.
1009 Tarlinton, R. P. Harvey, Homeodomain factor Nkx2-3 controls regional expression of
1010 leukocyte homing coreceptor MAdCAM-1 in specialized endothelial cells of the viscera.
1011 *Dev Biol*. **224**, 152–167 (2000).
1012 93. M. Nakache, E. Lakey Berg, P. R. Streeter, E. C. Butcher, The mucosal vascular addressin
1013 is a tissue-specific endothelial cell adhesion molecule for circulating lymphocytes. *Nature*
1014 *1989 337:6203*. **337**, 179–181 (1989).
1015 94. M. Briskin, D. Winsor-Hines, A. Shyjan, N. Cochran, S. Bloom, J. Wilson, L. M.
1016 McEvoy, E. C. Butcher, N. Kassam, C. R. Mackay, W. Newman, D. J. Ringler, Human
1017 mucosal addressin cell adhesion molecule-1 is preferentially expressed in intestinal tract
1018 and associated lymphoid tissue. *Am J Pathol*. **151**, 97 (1997).
1019 95. N. Ancellin, C. Colmont, J. Su, Q. Li, N. Mittereder, S.-S. Chae, S. Stefansson, G. Liau,
1020 T. Hla, Extracellular Export of Sphingosine Kinase-1 Enzyme. *Journal of Biological*
1021 *Chemistry*. **277**, 6667–6675 (2002).
1022 96. A. Cartier, T. Hla, Sphingosine 1-phosphate: Lipid signaling in pathology and therapy.
1023 *Science (1979)*. **366** (2019), doi:10.1126/SCIENCE.AAR5551/ASSET/C37AF20A-7636-
1024 40C9-A49A-4FC785158A19/ASSETS/GRAPHIC/366_AAR5551_FA.JPEG.
1025 97. J. Edsbagge, J. K. Johansson, F. Esni, Y. Luo, G. L. Radice, H. Semb, Vascular function
1026 and sphingosine-1-phosphate regulate development of the dorsal pancreatic mesenchyme.
1027 *Development*. **132**, 1085–1092 (2005).
1028 98. Y. He, B. Shi, X. Zhao, J. Sui, Sphingosine-1-phosphate induces islet β-cell proliferation
1029 and decreases cell apoptosis in high-fat diet/streptozotocin diabetic mice. *Exp Ther Med*.
1030 **18**, 3415 (2019).
1031 99. S. Majumder, M. Kono, Y. Terry Lee, C. Byrnes, C. Li, G. Tuymetova, R. L. Proia, A
1032 genome-wide CRISPR/Cas9 screen reveals that the aryl hydrocarbon receptor stimulates
1033 sphingolipid levels. *J Biol Chem*. **295**, 4341–4349 (2020).
1034 100. R. A. Brekken, E. H. Sage, SPARC, a matricellular protein: at the crossroads of cell-
1035 matrix. *Matrix Biol*. **19**, 569–580 (2000).
1036 101. C. L. Ryall, K. Viloria, F. Lhaf, A. J. Walker, A. King, P. Jones, D. Mackintosh, R.
1037 McNeice, H. Kocher, M. Flodstrom-Tullberg, C. Edling, N. J. Hill, Novel role for
1038 matricellular proteins in the regulation of islet β cell survival: the effect of SPARC on
1039 survival, proliferation, and signaling. *J Biol Chem*. **289**, 30614–30624 (2014).
1040 102. L. Hu, F. He, M. Huang, Q. Zhao, L. Cheng, N. Said, Z. Zhou, F. Liu, Y. S. Dai, SPARC
1041 promotes insulin secretion through down-regulation of RGS4 protein in pancreatic β cells.
1042 *Sci Rep*. **10**, 17581 (2020).
1043 103. L. W. Harries, L. J. McCulloch, J. E. Holley, T. J. Rawling, H. J. Welters, K. Kos, A Role
1044 for SPARC in the Moderation of Human Insulin Secretion. *PLoS One*. **8**, e68253 (2013).

104. L. Xu, F. Ping, J. Yin, X. Xiao, H. Xiang, C. M. Ballantyne, H. Wu, M. Li, Elevated Plasma SPARC Levels Are Associated with Insulin Resistance, Dyslipidemia, and Inflammation in Gestational Diabetes Mellitus. *PLoS One*. **8**, 81615 (2013).
105. H. O. Steinberg, G. Brechtel, A. Johnson, N. Fineberg, A. D. Baron, Insulin-mediated skeletal muscle vasodilation is nitric oxide dependent. A novel action of insulin to increase nitric oxide release. *Journal of Clinical Investigation*. **94**, 1172 (1994).
106. J. Almaça, J. Weitz, R. Rodriguez-Diaz, E. Pereira, A. Caicedo, THE PERICYTE OF THE PANCREATIC ISLET REGULATES CAPILLARY DIAMETER AND LOCAL BLOOD FLOW. *Cell Metab*. **27**, 630 (2018).
107. E. Blanco-Carmona, *bioRxiv*, in press, doi:10.1101/2022.02.28.482303.
108. G. Yu, D. K. Smith, H. Zhu, Y. Guan, T. T. Y. Lam, ggtree: an r package for visualization and annotation of phylogenetic trees with their covariates and other associated data. *Methods Ecol Evol*. **8**, 28–36 (2017).
109. S. Xu, M. Chen, T. Feng, L. Zhan, L. Zhou, G. Yu, Use ggbreak to Effectively Utilize Plotting Space to Deal With Large Datasets and Outliers. *Front Genet*. **12**, 2122 (2021).

Acknowledgments

Funding: We acknowledge funding from the Canadian Institutes of Health Research-JDRF, Team grant (CIHR - ASD 173662, JDRF - 5 SRA 2020 1058) (SSN, MCN, DD, GC, AP), Canada Foundation for Innovation (CFI), John R. Evans Leaders Fund (39909) (SSN), Canada First Research Excellence Fund, Medicine by Design, Team Project Award (MBD - MBDC2) (JZ, NH, C,TM, MCN, SSN), Early Researcher Award, Ministry of Research, Innovation and Science (ER17 13 14) (SSN), Natural Sciences and Engineering Research Council of Canada, Discovery Grant (RGPIN-201) (SSN)

Author contributions: STK and SSN conceptualized the study. SSN obtained funding for the study. STK curated, processed, analyzed and visualized all RNA sequencing data. NA and OC performed the sample collection, staining, imaging and acquisition of all *in situ* data. ST quantified all *in situ* data. SSN supervised the study. STK and SSN wrote the original manuscript. ST, SV, NA, OC were involved in reviewing and editing the manuscript.

Competing interests: Authors declare that they have no competing interests.

Data and materials availability: Available upon request.

Tables and Figures

Table 1. Summary of datasets used in this study

Dataset	Citation	Assay	Sequencing Method	Age
Descartes (Human)	Cao et al., Science, 2020(*26*)	Single Cell	Sci-RNA-seq3	Fetal
Tabula Muris (Mouse)	Tabula Muris Consortium (*25*)	Single Cell	SmartSeq2	Adult
Tosti – Adult (Human)	Tosti et al., Gastroenterology, 2021 (*31*)	Single Nuclei	10X Genomics	Adult

Tosti – Neonatal (Human)	Tosti et al., Gastroenterology, 2021 (*31*)	Single Nuclei	10X Genomics	Neonatal
Tabula Sapiens (Human)	Tabula Sapiens Consortium (*27*)	Single Cell	10X Genomics	Adult

1082
1083
1084
1085 **Table 2. Relevant gene lists**

Description	**Genes+**
Pancreas-specific EC gene signature derived from the overlap of *pancreas-enriched genes from the Tabula Muris and Descartes EC atlas and #endothelial-enriched genes from four pancreas datasets (Descartes, Tabula Muris, Tosti-Adult, Tosti-Neonatal)	*COL15A1, PLVAP, APLNR, GJA4 IGFBP3, HSPG2, RFLNB, BCAM, SOX4 CD34, MEOX1, ROBO4, NKX2-3 BHLHE40, CDC42EP1, AHR, ADAM15 CD81, EHD4, FAM129B, PDGFB, EBF3, ITGA6, PCDH17, MCAM, VWF, CLEC14A, MYO1C, JUP, TNFRSF1B, NEDD9 RNASE1, ACTN4, ITM2B, DCHS1, SYNPO, TIMP3, ENG, EGLN2, VAT1, NEURL1B MGAT1, MYH9, MMP15, CAVIN3, VAMP5 TBC1D1, CARD10, COL4A2, NID2 PODXL, AHNAK, HLA-E, MSN, GIT1 ARHGEF15, COL4A1, STOM, RAMP3, SHE, FKBP9, MGLL, SPRY1, TNFSF10, NFE2L1, GRN, HEG1, ITGA5, HDAC5, MMRN2, EFNA1, CASKIN2, LPAR6 , SPNS2, VCP, SNTB2, FMNL3, PKN1, RDX , RPS6KA2, NDST1, NOTCH1, SERINC3, TLN1, MCF2L, PLCB1, PXN*

1086 * Wilcoxon-rank sum test, log2FC > 0.25
1087 # Wilcoxon-rank sum test, log2FC > 0.25, Bonferroni-adjusted p-value <0.05
1088 + Genes in red also overlapped with significantly upregulated endothelial-specific,
1089 pancreas-enriched genes from the Tabula Sapiens EC atlas

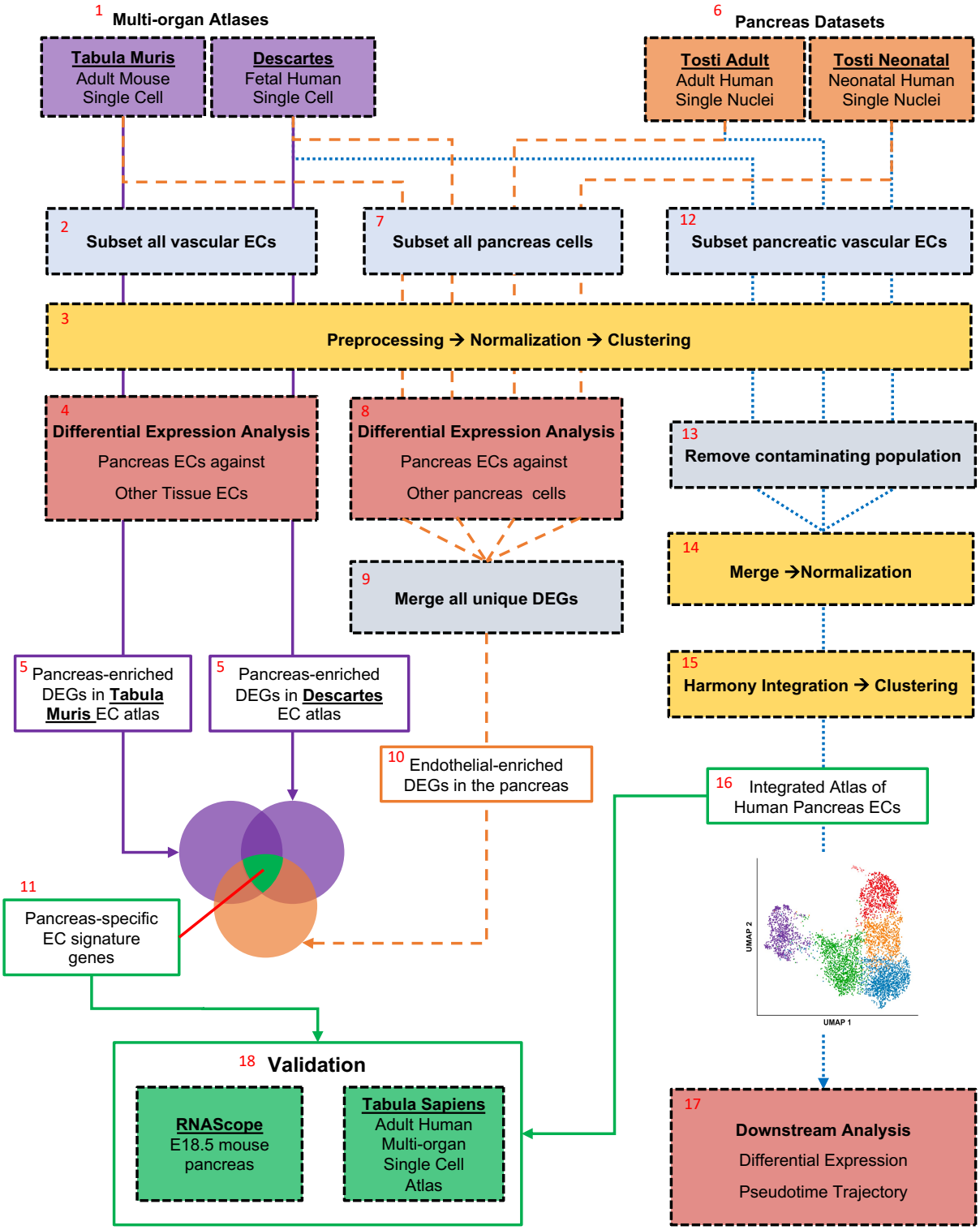

Figure 1. Analysis strategy to uncover a transcriptomic profile of pancreatic endothelial cells. This schematic summarizes the analysis conducted to obtain a biologically relevant pancreas-specific EC gene signature and a human pancreatic integrated atlas. Pancreas-specific EC signature genes lie at the overlap between pancreas-enriched differentially expressed genes (DEGs) derived from EC atlases and endothelial-enriched DEGS derived from pancreas datasets. Endothelial only atlases were derived from the human fetal Descartes and the adult mouse Tabula Muris multi-organ

gene expression atlases (1) by subsetting and pooling all vascular ECs from different organs (2). After preprocessing, normalizing and clustering (3), DEGs are identified between pancreas ECs against other tissue ECs (4) for each atlas (5). Next, two pancreas only datasets from Tosti et al (6) and all pancreas cells from the multi organ atlases were subsetted (7). After individually preprocessing, normalizing and clustering these pancreas datasets, DEGs were identified between pancreas ECs and other pancreas cells (8). These DEGs were merged (9) to produce a list of endothelial-enriched DEGs derived from pancreas datasets (10). The overlap of this list and the pancreas-enriched DEGs from the EC atlases produced the pancreas-specific EC genes (11). Next, to create an integrated atlas of pancreatic ECs, all pancreatic vascular ECs were subsetted (12) from the human pancreas dataset sources (Descartes and Tosti). These ECs were individually preprocessed, normalized and clustered. After which, contaminating clusters were removed (13). The remaining ECs were then merged and renormalized (14). The normalized counts were then integrated using Harmony (15), which produced the integrated pancreatic EC atlas (16). This atlas was used for further downstream analysis including DEG analysis within pancreatic EC subclusters and pseudotime trajectory analysis (17). Finally, the pancreas-specific EC gene signature (9) and populations of interest identified from the integrated atlas using Harmony (16) were validated *in silico* using the adult human Tabula Sapiens multi-organ gene expression atlas and *in situ* using RNAScope™ on embryonic day 18.5 (E18.5) mouse pancreatic tissue (18).

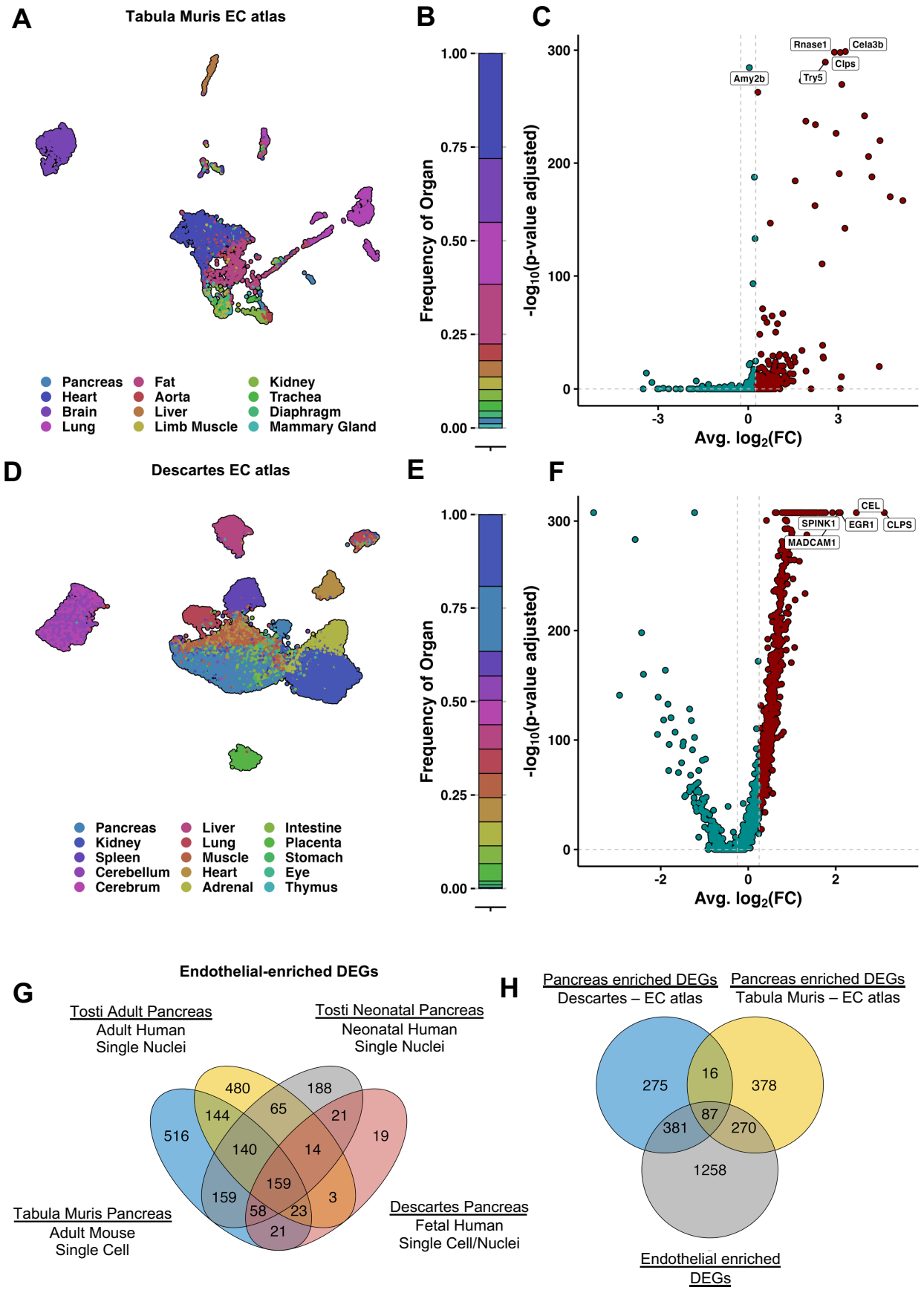
A
Tabula Muris EC atlas
Pancreas
Heart
Brain
Lung
Fat
Aorta
Liver
Limb Muscle
Kidney
Trachea
Diaphragm
Mammary Gland
B
Frequency of Organ
1.00
0.75
0.50
0.25
0.00
C
-log10(p-value adjusted)
Avg. log2(FC)
Rnase1
Cela3b
Clps
Try5
Amy2b
D
Descartes EC atlas
Pancreas
Kidney
Spleen
Cerebellum
Cerebrum
Liver
Lung
Muscle
Heart
Adrenal
Intestine
Placenta
Stomach
Eye
Thymus
E
Frequency of Organ
F
-log10(p-value adjusted)
Avg. log2(FC)
CEL
SPINK1
EGR1
CLPS
MADCAM1
G
Endothelial-enriched DEGs
Tosti Adult Pancreas
Adult Human
Single Nuclei
Tosti Neonatal Pancreas
Neonatal Human
Single Nuclei
Tabula Muris Pancreas
Adult Mouse
Single Cell
Descartes Pancreas
Fetal Human
Single Cell/Nuclei
480
188
144
65
21
516
19
140
14
159
159
3
58
23
21
H
Pancreas enriched DEGs
Descartes – EC atlas
Pancreas enriched DEGs
Tabula Muris – EC atlas
275
16
378
87
381
270
1258
Endothelial enriched
DEGs

1115

1116 **Figure 2. Determining a biologically relevant pancreas-specific endothelial cell (EC) gene**
1117 **signature .** A-F) shows the summary of EC atlases derived from the Tabula Muris (A-C) Descartes
1118 (D-F). A) and D) shows the UMAP visualization of single cell sequencing data for the ECs from
1119 all available organs. B and E) Highlight the tissue/organ ratios in the EC atlases and the colors
1120 correspond to the labelling in the preceding UMAPs. C and F) are volcano plots demonstrating
1121 differentially expressed genes (DEGs) in pancreas ECs against other organ/tissue ECs. Enriched
1122 DEGs (log2FoldChange > 0.25; Wilcoxon Rank Sum Test) are shown in red and the rest of the
1123 DEGs in blue. Further, the top 5 significant DEGs are labeled. G) shows the overlap of significant
1124 endothelial marker DEGs (log2FoldChange > 0.25; Wilcoxon Rank Sum Test, Bonferroni-adjusted
1125 p-value < 0.05) derived from four different pancreas single cell/nuclei gene expression datasets
1126 (Tabula Muris, Descartes, adult and neonatal pancreas from Tosti et al.). Endothelial marker DEGs
1127 are defined as DEGs upregulated in vascular ECs in the pancreas compared to all other pancreas
1128 cell-types. Merging all unique DEGs from the different datasets produced the list of "endothelial-
1129 enriched DEGs". H) shows the overlap of pancreas-enriched DEGs (log2FoldChange > 0.25;
1130 Wilcoxon Rank Sum Test, Bonferroni-adjusted p-value < 0.05) derived from EC atlases obtained
1131 from the human fetal Descartes and adult mouse Tabula Muris gene expression atlas, and the
1132 previously derived merged list of endothelial-enriched DEGs. The overlap of all these sets produces
1133 the "pancreas-specific EC gene signature".

1134

1135

1136

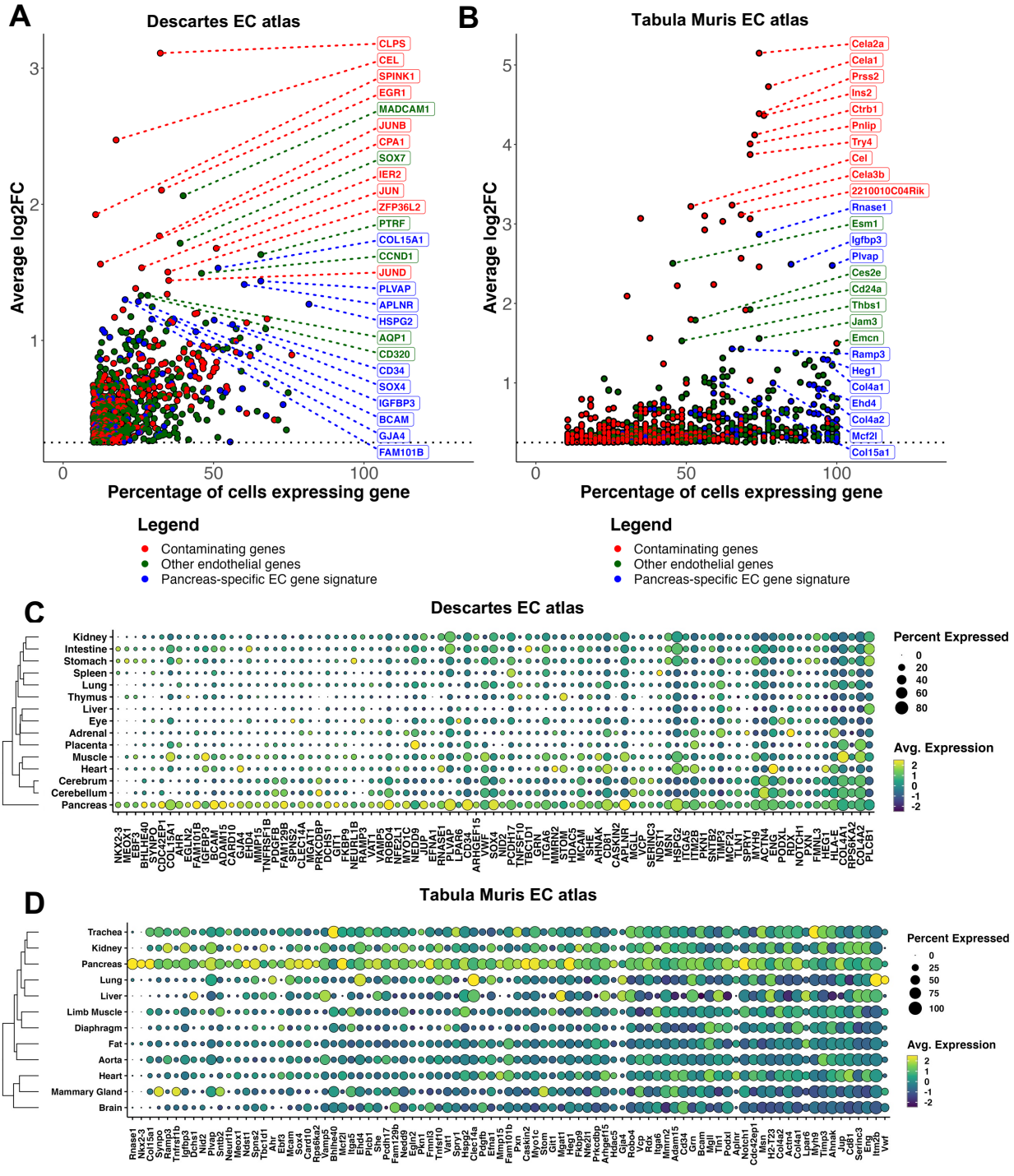

Figure 3. Assessment of the pancreas-enriched DEGs in the Descartes and Tabula Muris endothelial cell (EC) atlases. A) and B) demonstrate a scatterplot for all significant (log2FoldChange > 0.25; Wilcoxon Rank Sum Test, Bonferroni-adjusted p-value < 0.05) pancreas-enriched DEGs identified from the Descartes and Tabula Muris EC atlases. The y-axis is average log2FC of gene expression in the pancreas ECs vs other tissue ECs and the x-axis is percentage of ECs expressing the gene. Potential contaminating genes, are colored in red, pancreas-specific EC signature genes are in blue and the rest of the endothelial-enriched genes are in green. C) and D) demonstrates the individual average scaled log-normalized expression of the pancreas-specific EC signature genes in the Descartes and Tabula Muris EC gene expression atlas, respectively. Genes

1147 are ordered in decreasing order based on the fold-change in percentage of ECs expressing gene in
1148 the pancreas against other tissues/organs. Pancreas-specificity of this signature is demonstrated
1149 using hierarchical clustering of genes based on Euclidian distances between the average scaled
1150 expression of the DEGs across the different tissues/organs.

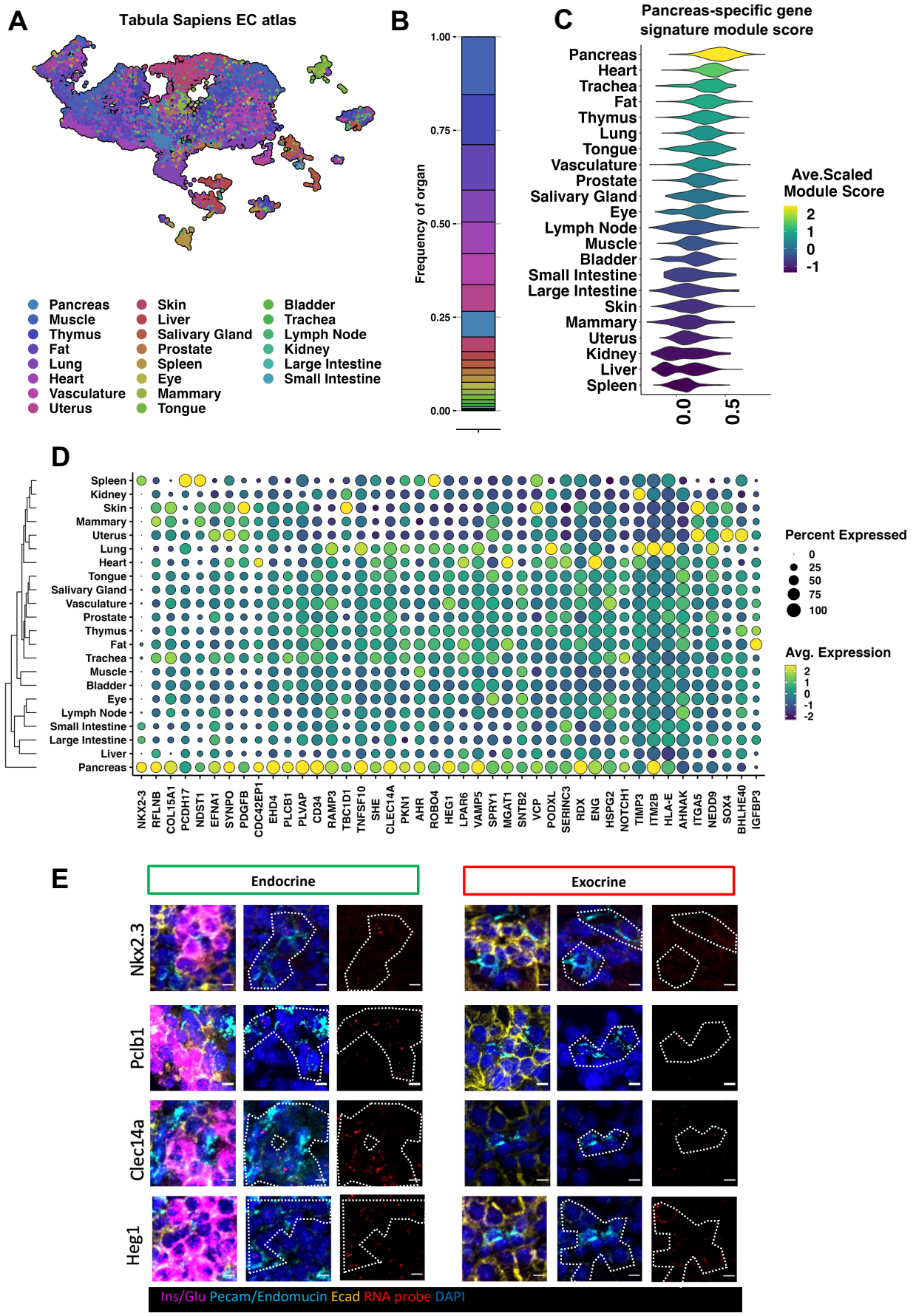
A
Tabula Sapiens EC atlas
Pancreas
Muscle
Thymus
Fat
Lung
Heart
Vasculature
Uterus
Skin
Liver
Salivary Gland
Prostate
Spleen
Eye
Mammary
Tongue
Bladder
Trachea
Lymph Node
Kidney
Large Intestine
Small Intestine
B
Frequency of organ
1.00
0.75
0.50
0.25
0.00
C
Pancreas-specific gene signature module score
Pancreas
Heart
Trachea
Fat
Thymus
Lung
Tongue
Vasculature
Prostate
Salivary Gland
Eye
Lymph Node
Muscle
Bladder
Small Intestine
Large Intestine
Skin
Mammary
Uterus
Kidney
Liver
Spleen
0.0
0.5
Ave.Scaled Module Score
2
1
0
-1
D
Spleen
Kidney
Skin
Mammary
Uterus
Lung
Heart
Tongue
Salivary Gland
Vasculature
Prostate
Thymus
Fat
Trachea
Muscle
Bladder
Eye
Lymph Node
Small Intestine
Large Intestine
Liver
Pancreas
NKX2-3
RFLNB
COL15A1
PCDH17
NDST1
EFNA1
SYNPO
PDGFB
CDC42EP1
EHD4
PLCB1
PLVAP
CD34
RAMP3
TBC1D1
TNFSF10
SHE
CLEC14A
PKN1
AHR
ROBO4
HEG1
LPAR6
VAMP5
SPRY1
MGAT1
SNTB2
VCP
PODXL
SERINC3
RDX
ENG
HSPG2
NOTCH1
TIMP3
ITM2B
HLA-E
AHNAK
ITGA5
NEDD9
SOX4
BHLHE40
IGFBP3
Percent Expressed
0
25
50
75
100
Avg. Expression
2
1
0
-1
-2
E
Endocrine
Exocrine
Nkx2.3
Pclb1
Clec14a
Heg1
Ins/Glu Pecam/Endomucin Ecad RNA probe DAPI

1151

1152 **Figure 4. Validating the pancreas-specific endothelial cell (EC) gene signature in a third**
1153 **independent endothelial atlas obtained from the Tabula Sapiens gene expression atlas.** A)
1154 shows a UMAP of all organ ECs in the Tabula Sapiens atlas (left) and also highlights only the
1155 pancreas ECs within this UMAP (right). B) shows the ratios of ECs from each organ/tissue and is
1156 colored corresponding to the preceding UMAP legend. C) demonstrates the module scores derived
1157 by assessing the collective expression of the pancreas-specific endothelial cell (EC) gene signature
1158 using Seurat's AddModuleScore function in the different EC populations of the Tabula Sapiens EC
1159 atlas. Each violin is colored based on the average scaled module score for that cluster. D)
1160 demonstrates the individual log-normalized average scaled expression of the pancreas-specific EC
1161 signature genes in the Tabula Sapiens EC atlas. Hierarchical clustering based on Euclidian
1162 distances between the average scaled expression of the DEGs across the different tissues
1163 demonstrates specificity to the pancreas. E) demonstrates *in situ* images of E18.5 mouse pancreas
1164 tissue bound by RNAscope™ probes (red) for selected pancreas-specific EC genes. Endocrine and
1165 exocrine regions are identified by immunofluorescence (IF) co-staining of insulin and glucagon
1166 (pink), which stains cells of the islets; vasculature is identified by co-staining of pecam-1 and
1167 endomucin (neon); all other epithelial cells are stained by e-cadherin (yellow); and the nuclei are
1168 stained by DAPI (blue). The white dotted outline demonstrates manually outlined regions rich in
1169 pecam1-endomucin co-staining. Scale bars correspond to 5 μm.

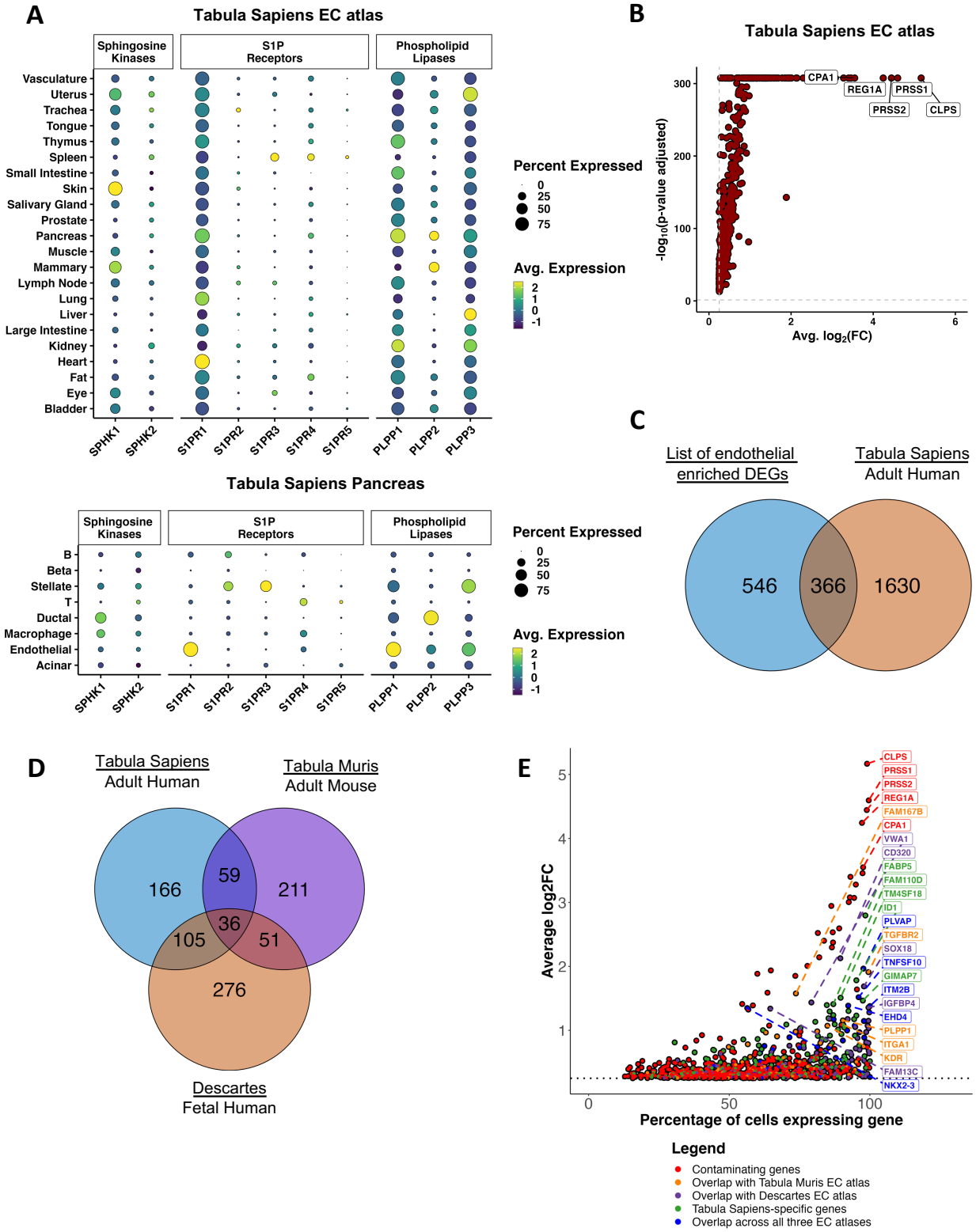

Figure 5. Assessment of the pancreas-enriched differentially expressed genes in the Tabula Sapiens atlas. A) demonstrates the average expression of key sphingosine-1-phosphate associated molecules in the Tabula Sapiens EC atlas (top) and in the the Tabula Sapiens pancreas dataset (bottom). B) demonstrates volcano plots for the Tabula Sapiens atlas, highlighting only upregulated significant (log2FoldChange > 0.25; Wilcoxon Rank Sum Test, Bonferroni-adjusted p-value <

0.05) differentially expressed genes (DEGs) enriched in pancreas ECs against other tissue ECs. The x-axis is average log2FC of the gene and the y-axis is –log10 of adjusted p-value. Top 5 DEGs are highlighted. C) demonstrates overlap of all pancreas-enriched significant DEGs derived from the Tabula Sapiens EC atlas and a list of endothelial-enriched DEGs curated for this study from four different pancreas datasets across different age and species. D) demonstrates the overlap of all pancreas-enriched DEGs obtained from the Tabula Sapiens EC atlas with the curated list of endothelial-enriched DEGs. E) demonstrate a scatterplot for all significant (log2FoldChange > 0.25; Wilcoxon Rank Sum Test, Bonferroni-adjusted p-value < 0.05) pancreas-enriched DEGs identified from the Tabula Sapiens EC atlas. The y-axis is average log2FC of gene expression in the pancreas ECs vs other tissue ECs and the x-axis is percentage of ECs expressing the gene.

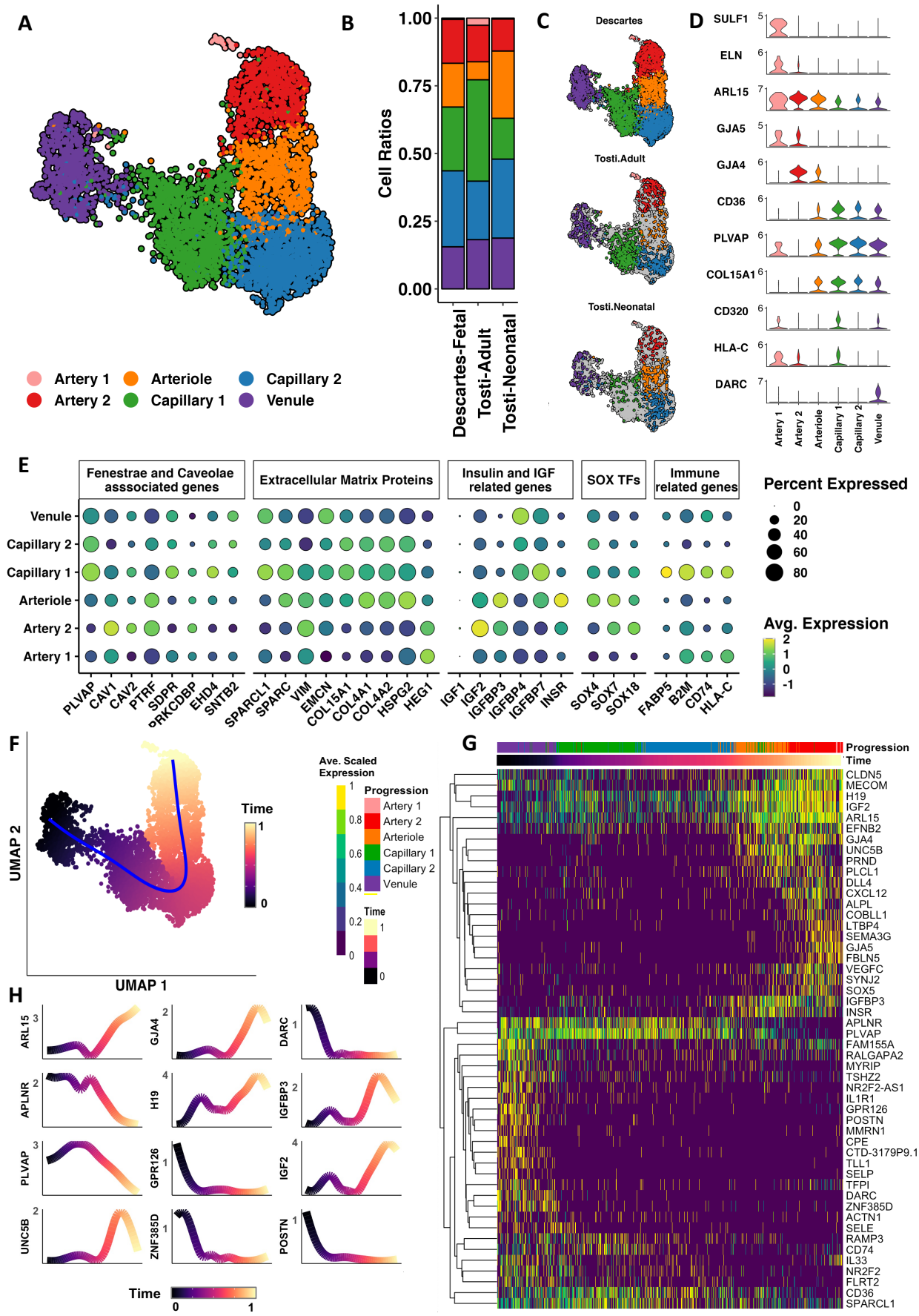
A
Artery 1
Artery 2
Arteriole
Capillary 1
Capillary 2
Venule
B
Cell Ratios
1.00
0.75
0.50
0.25
0.00
Descartes-Fetal
Tosti-Adult
Tosti-Neonatal
C
Descartes
Tosti.Adult
Tosti.Neonatal
D
SULF1
ELN
ARL15
GJA5
GJA4
CD36
PLVAP
COL15A1
CD320
HLA-C
DARC
Artery 1
Artery 2
Arteriole
Capillary 1
Capillary 2
Venule
E
Fenestrae and Caveolae asssociated genes
Extracellular Matrix Proteins
Insulin and IGF related genes
SOX TFs
Immune related genes
Venule
Capillary 2
Capillary 1
Arteriole
Artery 2
Artery 1
PLVAP
CAV1
CAV2
PTRF
SDPR
PRKCDBP
EHD4
SNTB2
SPARCL1
SPARC
VIM
EMCN
COL15A1
COL4A1
COL4A2
HSPG2
HEG1
IGF1
IGF2
IGFBP3
IGFBP4
IGFBP7
INSR
SOX4
SOX7
SOX18
FABP5
B2M
CD74
HLA-C
Percent Expressed
0
20
40
60
80
Avg. Expression
2
1
0
-1
F
UMAP 2
UMAP 1
Time
1
0
Ave. Scaled Expression
Progression
Artery 1
Artery 2
Arteriole
Capillary 1
Capillary 2
Venule
Time
G
Progression
Time
CLDN5
MECOM
H19
IGF2
ARL15
EFNB2
GJA4
UNC5B
PRND
PLCL1
DLL4
CXCL12
ALPL
COBLL1
LTBP4
SEMA3G
GJA5
FBLN5
VEGFC
SYNJ2
SOX5
IGFBP3
INSR
APLNR
PLVAP
FAM155A
RALGAPA2
MYRIP
TSHZ2
NR2F2-AS1
IL1R1
GPR126
POSTN
MMRN1
CPE
CTD-3179P9.1
TLL1
SELP
TFPI
DARC
ZNF385D
ACTN1
SELE
RAMP3
CD74
IL33
NR2F2
FLRT2
CD36
SPARCL1
H
ARL15
GJA4
DARC
APLNR
H19
IGFBP3
PLVAP
GPR126
IGF2
UNC5B
ZNF385D
POSTN
Time
0
1

1186

Figure 6. Integrated map of human pancreatic endothelial cells (ECs). Three different human pancreatic EC datasets were derived from their parent data and integrated using Harmony. This includes the fetal human pancreas dataset from the Descartes gene expression atlas and the neonatal and adult pancreas dataset from Tosti et al. A) shows the resulting integrated UMAP using the harmony transformed principle component values. B) Shows the percentage distribution of different subpopulations in each dataset colored according to the labelling of the preceding UMAP. C) shows the UMAP of the integrated map split by dataset (Descartes-Fetal, Tosti-Adult, Tosti-Neonatal). D) demonstrates violin plots showing expression of markers used to annotate different clusters in the integrated atlas. F) shows the UMAP of the integrated map colored by pseudotime inferred through trajectory analysis using SCORPIUS. The trajectory is colored in blue. G) shows the heatmap demonstrating the change in average scaled expression of the top 50 unique markers determined by Wilcoxon Rank Sum Test for each subcluster across pseudotime. Genes are hierarchically clustered based on the Euclidian distance between the average scaled expression of the genes. H) Shows the expression of the top 12 genes across pseudotime ranked by importance to trajectory interference using SCORPIUS.

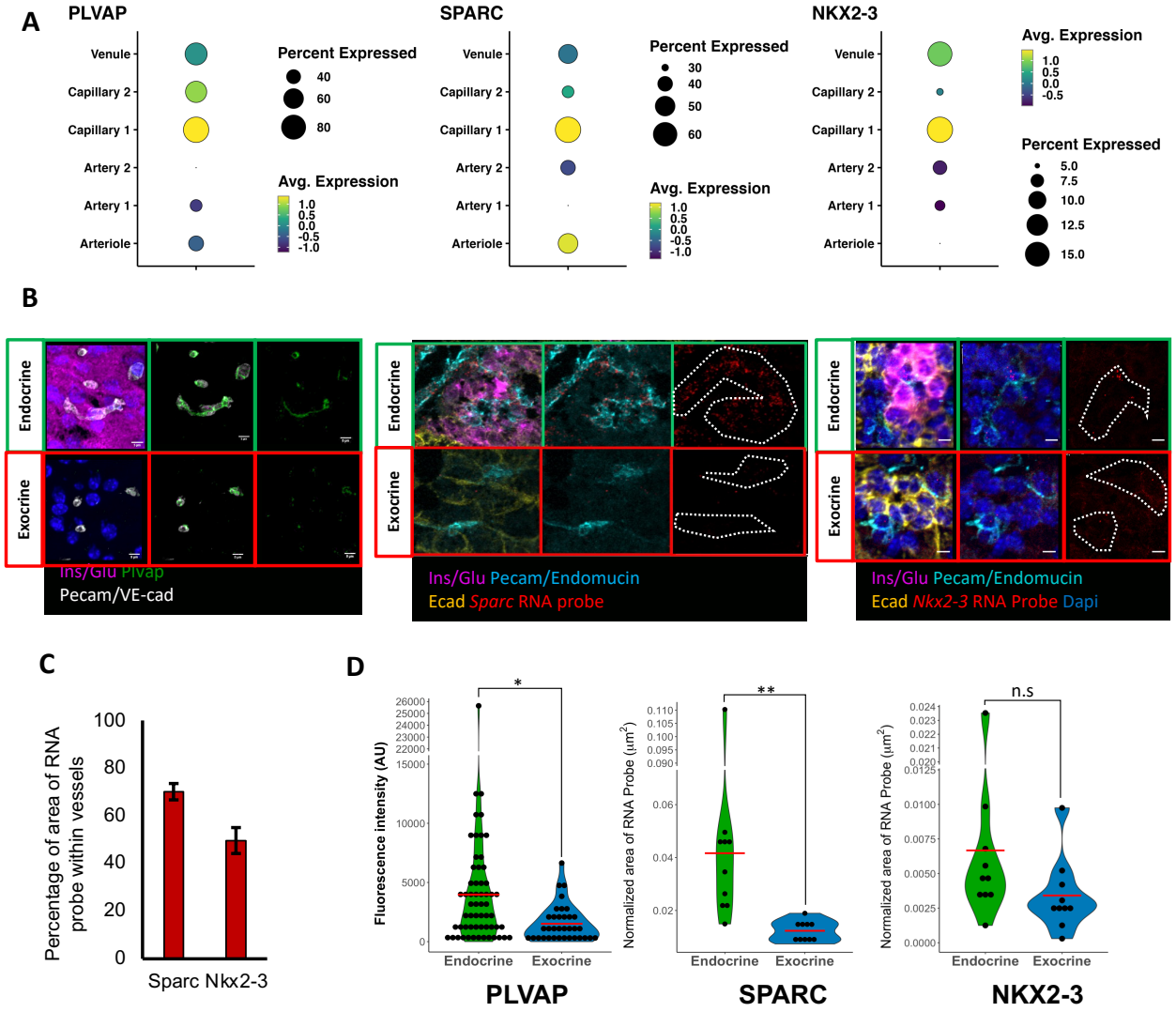

Figure 7. *In situ* validation of islet-specific EC capillary population. A) demonstrates the expression of 3 different DEGs that were enriched in the capillary 1 population of the integrated EC atlas. These genes include *PLVAP* (left), *SPARC* (middle) and *NKX2-3* (right). D-F)

demonstrate *in situ* validation of the 3 selected capillary 1 DEGs on E18.5 mouse pancreatic tissue cross-sections using RNAScope™ and Immunofluorescence (IF) staining. D) demonstrates representative images taken of microvessels in exocrine and endocrine regions for IF staining (green) of Plvap (left) and RNAscope™ probe staining (red) for *Sparc* (middle) and *Nkx2-3* (right) in tissue cross-sections. Pink shows IF co-stain of glucagon and insulin, which highlights the islets from the exocrine tissue for all images; green for Plvap IF and red for *Sparc* and *Nkx2-3* RNA probes. Images highlight microvessels co-stained with Pecam1 and endomucin; yellow shows E-cadherin staining. The scale bar represents 5 μm. E) shows the average percentage of probe bound within microvessels outlined by a blinded researcher based on only Pecam1/endomucin IF staining across all tissue cross-sections. F) Demonstrates quantification of fluorescence intensity in arbitrary units (AU) for Plvap and RNAscope™ area of probe binding (μm^2) for *Sparc* and *Nkx2-3* in endocrine and exocrine microvessels, where each vessel was considered 1n. One-tailed t-test statistics was used to calculate significance (* - p-value <0.05, ** - p-value <0.01, *** - p-value <0.001).